DEVELOPMENT AND APPLICATION OF A TECHNIQUE FOR STEADY STATE AERODYNAMIC HEAT TRANSFER MEASUREMENTS

Thesis by

Frederic W. Hartwig

In Partial Fulfillment of the Requirements

For the Degree of

Doctor of Philosophy

California Institute of Technology

Pasadena, California

1957

ACKNOWLEDGMENTS

The author wishes to express his sincere appreciation to his advisor, Professor Lester Lees, for his assistance, guidance, and encouragement during this work. A great debt of thanks is due Mr. Howard McDonald and Mr. C. A. Bartsch without whose skill, patience, and cooperation the model instrumentations used could never have been developed. The author wishes to extend his gratitude to Dr. H. T. Nagamatsu for the initiation and early suggestions on this project. And finally the author wishes to thank Captain Robert Slizeski for his assistance during the testing and calibration phases of this effort.

ABSTRACT

A technique was developed for measuring steady state heat transfer on a hemisphere cylinder and the results are compared with theory. The instrumentation consisted of a miniaturized thermopile of silver-constantan thermocouples approximately 1/8" x 1/16" x 1/100". The repeatability of readings with this device was found to be excellent. These heat measuring devices, or heat meters, were installed in both a ceramic hemisphere cylinder and in a similar metal one. There were obtained three different heat flow rates at each of six different combinations of tunnel pressure and temperature.

The results compared very well with a theory developed by Lester Lees based upon the assumption of local similarity.

TABLE OF CONTENTS

LIST OF SYMBOLS

The subscript "w" refers to gas properties evaluated at the local surface temperature, while the subscript "e" denotes quantities at the outer edge of the boundary layer, and the subscript "∞" refers to ambient properties just ahead of the bow shock wave. The subscript "o" generally denotes quantities at the forward stagnation point. The subscript "a" indicates adiabatic conditions. A prime denotes differentiation with respect to η.

a	speed of sound
C_p	specific heat at constant pressure
D	diameter
g	h_s/h_{s_e}
h	static enthalpy
h_s	total enthalpy
k	coefficient of thermal conductivity
M	Mach number, u/a
p	static pressure
p_o'	stagnation pressure behind normal shock
Pr	Prandtl number, $C_p\mu/k$
$\dot{q}$	local heat transfer rate
r_o	radius of cross-section of body of revolution
R_o	nose radius
R	gas constant for air
s	distance along body surface, measured from forward stagnation point

I. INTRODUCTION

Steady-state aerodynamic heat-transfer measurements have always presented severe difficulties. When pairs of thermocouples are used to measure the temperature gradient in a solid body, the differential millivolt output is usually quite low, unless the two thermocouples are spaced reasonably far apart. But the heat flux is generally not normal to the surface because of axial temperature gradients in the material, and the corrections required to obtain the normal heat flux are often as large as 50 to 100 per cent of the measured values. In an attempt to avoid these difficulties, a device has been constructed which allows the distance between the thermocouple pair to be greatly reduced while the required millivolt output for a given heat flow is maintained.

The purpose of this experiment was to apply these devices to an actual model and to compare the results with theoretically predicted heat rates. In this manner the new technique can be properly evaluated.

II. EQUIPMENT AND PROCEDURE

A. Equipment

1. Wind Tunnel Description

The heat transfer experiments were conducted in the original Leg 2 of the GALCIT hypersonic facility, which has since been replaced by an improved version. This tunnel is of a continuous flow, closed-return type with a nominal Mach number of 7.8 and a test section size of 5 x 6.5 inches. The stagnation pressure (p_o) ranges between 100 psig and 350 psig to within accuracy limits of $\pm$ 2 psig. The stagnation temperature (T_o) ranges between 300°F and 800°F within limits of $\pm$ 5°F. This tunnel uses the same power plant and compressor system as Leg 1 of the GALCIT hypersonic facility. A complete description of the compressor plant and the associated instrumentation may be found in References 12 and 13. Associated instrumentation includes self-balancing millivolt meters, mercury and silicone manometer banks, and a schlieren optical system.

2. Instrumentation

a. Heat Meters

The heat meters are thermocouples located on top and bottom of a thin glass sheet so as to measure the temperature on the two surfaces. As heat flows through the glass a temperature difference, ΔT, is set up proportional to the rate of heat flow. This difference in temperature is sensed by the thermocouples and can be read on a millivolt meter. By proper calibration these millivolt readings can

be interpreted in terms of the corresponding heat flow rates.

Since it is desirable to measure the heat rate right at the surface in order to avoid problems arising from axial temperature gradients, the glass sheet must be made as thin as possible. In this case it was .007" thick. Since the glass is very thin the ΔT across it is small, and hence the millivolt output per pair of thermocouples is low. Therefore, the thermocouples were so wired as to have 50 pairs in series. It is also desirable to measure the heat flow at a point, so over-all meter size was kept to 1/8" x 1/16" x 1/100" which imposed a difficult manufacturing problem. Therefore, a short discussion of construction technique is included. (See Appendix A.)

b. Thermocouples

Surface temperatures must be measured at the same time as heat transfer measurements are being made. Since space on the model surface is limited a technique of making surface thermocouples which occupy a minimum of space was developed. Constantan wire .001" in diameter was laid on the surface of each model from nose to rear. The wire was then coated with a thin solution of low melting silicate flux and fired at 1100°F. This flux thus bonded the wire to the surface under a thin glass-like coating less than .001" thick. This coating was removed at regular and precisely-located points by making a cut with a knife blade. The exposed wire was contacted with silver paint so that a silver constantan thermocouple junction was formed at each cut. The silver paint formed a lead which was extended to the rear of the model where it connected with a silver wire leading out of the tunnel from the rear of the model to a millivolt

meter. In like manner the constantan "common" wire was brought out to the millivolt meter. Thus there was a constantan lead common to all thermocouples and a silver lead for each different thermocouple. (See Figure 1a. Base lead-in wires are not shown in this photograph.)

3. Model Description

a. Ceramic Model

Because of their small size, it was felt that the heat meters might not have enough sensitivity to give a reasonable output for the heat transfer rates expected. As described in Section 2.a the heat meter output in millivolts is proportional to the ΔT across it. Now for a given heat transfer rate, ceramic with its low thermal conductivity has a larger ΔT per unit thickness than a metal, say, with a high thermal conductivity. Therefore, the heat meter sensitivity will be larger if it is imbedded in a ceramic material. The model itself was of a ceramic of high strength and so manufactured as to give uniform wall thicknesses of .0625". A few models were broken to check on this uniformity, and the largest variation detected was $\pm$ .002". Although this dimension has no bearing on the measurements made in this experiment, this accuracy is mentioned because it is felt it represents a very remarkable manufacturing achievement. The model was supported by a sting containing coaxial inflow and outflow water pipes. Also inside the sting were the 31 wires for instrumentation. The model was 1.75" in diameter and 5.75" in length.

b. Metal Model

The metal model was made to avoid the breakage problem associated with the ceramic model and also to give different heat rates. It was of steel and machined to such a size as to duplicate the ceramic model, except that 5 more heat meters were installed in the nose region. The advantage of using ceramic material, as already discussed, was realized also in the metal model by coating the model with a .020" layer of porcelain and imbedding the meter in this layer. It was subsequently discovered that meter sensitivity was more than adequate and in the region of the stagnation point, meter size was reduced to 18 turns.

c. Installation of Heat Meters

Small indentations of meter size were molded into the ceramic model during manufacture. Similar indentations were ground into the porcelain coating of the metal models. The meters were cemented into these indentations, and the surface was made aerodynamically smooth. The leads from each meter were exposed to the surface, and contact was made to them with silver conductor paint. These painted leads were brought to the rear of the model where they connected with the lead wires to the millivolt meter. (See Figure 1b. This particular model is without lead-in wires and the model surface shows discoloration from a test made at a later date with an internal heater.)

d. Pressure Model

A brass model was constructed following standard pressure model techniques with three taps located at 45° from the nose and equally spaced around the axis for the purpose of making accurate alignment of the model along the flow axis. The other pressure taps were located from nose to rear in a spiral. Pressures near the nose were read on a mercury manometer and all other pressures were read on a silicone manometer.

B. Procedure

1. Calibration

a. Thermocouples

Since a silver-constantan thermocouple curve of temperature versus millivolts was not available, it was necessary to calibrate the thermocouples. This calibration was accomplished by making thermocouples of the same materials on glass rods. In addition, one of the ceramic models containing 16 thermocouples was calibrated. A container of oil was heated to a stable temperature, and the temperature was measured at several positions in the bath using thermometers and standardized copper-constantan thermocouples. The bath was stirred to help remove convection effects. The thermocouples were placed at several positions in the bath, and an average reading was taken. When the model was calibrated the maximum variation in the 16 thermocouples was less than 1 per cent. For high temperature calibration (above 550°F) a salt bath was used. This

procedure required that the thermocouples be placed on the inside of a test tube before immersion so as to avoid a battery effect created by the salt and the two dissimilar metals. Nevertheless, calibration became less accurate above 500°F. (See Figure 5.)

b. Heat Meters

The calibration of the heat meters was the key to the success of the whole experiment. Therefore, much care and time were spent upon this problem.

Since slight variations in installation from one meter to the next could cause variations in sensitivity it was necessary to calibrate the meters after installation in the model. An oven was constructed whose heating elements duplicated, at a larger radius, the shape of the model. (See Figure 6.) Then a $\frac{1}{2}$-inch thick copper shell was machined to fit between the heaters and the model and act as a uniform heat source for the model. The space between the model and copper shell was 1/8 inch. The oven was capable of a continuous dissipation rate of 10,000 watts/ft.^{2} of model area. At the lower heat flow rates up to 1/3 maximum, it was possible to fill the gap between the model and the copper shell with oil and heat the model by conduction. Above this point the oil temperature was excessive, so the oil was removed, and radiant heat transfer was used. Beyond about 2/3 maximum oven output the heater wire became too hot and it was necessary to remove the copper shell so that the heater wires themselves could radiate directly to the model. This last step, suggested by H. W. Liepmann, was possible because the heater wires were very uniformly distributed and were almost one inch from the model

surface, which meant that no individual meter would be able to "focus" on any particular hot spot, but rather would "see" a uniform source of radiant heat. Judging by the uniformity of the model surface temperature during calibration this assumption was very well justified. In the future it is suggested that any such ovens be constructed using the heater element itself as the radiator.

Since the oil conduction method requires that the spacing of the model in the oil bath from the copper be very precise, it was necessary to provide spacers. Also, the oil bath tends to set up very strong convection currents even with a spacing of only 1/8 inch. Fortunately a solution to both these problems was found by using silicone rubber "O" rings as spacers. By filling as much of the available space between the model and the copper shell as possible with these spacers convection currents were blocked. The thermal conductivities of the silicone rubber and of the vegetable oil used were identical.

The losses in such a calibration apparatus must be prevented or measured accurately. The heater wires were backed by stainless steel reflector sheets. Outside of these sheets were three layers of 1/4 inch asbestos sheet. This package was then placed in a large box and the remaining space, about 4 inches, filled with rock wool. On the outside of the box were commerical heat meters which measured the loss through the walls. This loss was taken into account in the calibration, although it never exceeded 5 per cent of the total input.

On the top of the oven, where the model entered, the problem was more difficult. The lid for the oven was made of a thin flat ring of Transite of a proper size to close the oven and still let the model enter. This ring was wrapped with constantan wire appropriately

silver plated so as to form a heat meter. On top of this ring was placed another ring, this time wrapped with nichrome wire so as to form a bucking heater. The input to this heater was constantly adjusted so as to maintain zero output on the heat meter oven lid. Thus it was assumed there were no losses out of the top.

The model was rotated to three different positions while in the oil bath. During the radiant calibration the model was run in both the vertical and horizontal position. Input was measured with a watt meter and output read on a Brown millivolt meter. No reading was taken until the output remained constant for 20 minutes. By knowing model area exposed to the heater, (0.1596 ft.^{2}) and power input (less losses out the box walls) a heat rate in BTU/ft.^{2}/hr. can be evaluated for any given heat meter output in millivolts. (See Figure 7 for a typical calibration curve.)

Since meter sensitivity is a function of absolute temperature, it is necessary to make certain that the coolant flow duplicates tunnel conditions so that the meters will be calibrated at the same temperature level as that at which they will be operating in the tunnel. This condition was satisfied for the ceramic model and the water-cooled metal model but not for the air cooled metal model. However, the variation of the meter sensitivity with temperature is known both from commerical sources and by calculation from the slope of the thermocouple calibration curve, so that a simple correction could be made to the air cooled metal model readings.

2. Testing

In order to determine the maximum model size that could be tested in the hypersonic tunnel, six dummy models were built with diameters ranging from 3/4 inch to 2-1/4 inch. It was just possible to start the tunnel with the 2-1/4 inch model. Earlier surveys of the tunnel flow by T. Kubota showed that there was a core of uniform flow approximately 3 inches in diameter, and it was decided that a two-inch model would be used. However, after the installation of lead-in wires on the base of the model, the flow would not start, and it was necessary to decrease the model diameter to 1.75". The length of the model was chosen by observing that the reflected shock would strike a 2-inch model at a distance of about nine inches from the nose. T. Kubota ran a boundary layer profile study on a long hemisphere cylinder at these tunnel conditions and found no indication of transition as far back as six diameters. (The Re based upon model diameter and conditions behind the shock is of the order of 30,000 per inch.) Therefore, a model length of 5.75 inches was chosen.

Correct evaluation of T_o in the test section is essential to this experiment. Therefore a comparison was made between the T_o indicated by a thermocouple in the settling chamber and T_o in the test section. It was not possible to obtain true test section T_o at the nose of the model even with no internal cooling, because of axial conduction. Therefore, it was necessary to place a thermocouple in the flow in such a manner as to measure T_o and yet not be affected by conduction errors. It was observed that the shock wave stood out from the nose a distance of about 1/8 of an inch. (See Figure 2.) Since this flow region

is subsonic, the adiabatic surface temperature should be very nearly equal to the true stagnation temperature. Therefore, a small iron-constantan thermocouple was installed on the nose of one of the ceramic models so that its bead extended about 1/16" ahead of the nose and into the subsonic region behind the shock. (This small bead can be seen on the model nose in Figure 1a.) The difference between tunnel indicated T_o and the measured test section T_o was never more than 4^oF, which is within the accuracy of the tunnel temperature control. No correction was made for this difference in T_o.

The ceramic model was run at p_o = 300 psig. and 200 psig., and $T_o = 505^oF$, 600^oF, and 700^oF on each of three different days. The metal model was run water-cooled at the same tunnel conditions for four days and then, after calibration, it was run again for a fifth day. The same model was run air-cooled for three days. After all the tests were completed an attempt was made to heat this model internally in order to reverse the direction of heat flow, but the cement holding the meters in the model began to deteriorate at the high temperatures involved. (See Figure 1b.) The pressure model was run at the above tunnel conditions for one day only. (See Figure 8.)

No readings were taken until all tunnel conditions showed no change for 20 minutes even though meter response time seemed to be much less than one second.

The coolant water flow was approximately one quart per minute, and the return flow temperature rise was less than 5^oF.

T. Kubota has determined that the minimum temperature in this tunnel to avoid free stream condensation is $T_o = 700^oF$. However,

the pressure distribution on a blunt body was not appreciably affected by lowering T_o to 600°F. At T_o = 505°F it is probable that condensation affects both the pressure distribution and the heat transfer rate distribution.

III. THEORY

In the present experiments the variation in surface enthalpy over the body is small compared with the average value of the "driving potential", $h_{aw} - h_w$. In such cases the concept of local similarity furnishes a useful approximation for the surface heat transfer rate distribution (Reference 2). In this method a transformation of coordinates is introduced which replaces s (distance measured along surface from nose) and y (distance measured normal to the surface) by $\tilde{s}$ and η, where $\tilde{s}$ and η are defined by the relations

$$\tilde{s} = \int_0^s \rho_e \mu_e u_e r_o^2 \, ds$$

and

$$\eta = \frac{\rho_e \mu_e}{(2\tilde{s})^{\frac{1}{2}}} \int_0^y r_o \, (\rho/\rho_e) \, dy \quad .$$

Thus

$$\dot{q} = k \left(\frac{\partial T}{\partial y} \right)_w = \frac{\mu_w \rho_w u_e r_o h_{s_e}}{Pr \ (2\tilde{s})^{\frac{1}{2}}} \ (g')_w \ , \qquad (1)$$

(See Reference 2.)

where the subscripts w and e indicate that the physical quantities concerned are evaluated at the wall and outer edge of the boundary layer, respectively. The quantity g is defined as the total enthalpy ratio h_s/h_{s_e}, and the prime indicates differentiation with respect to η. The quantity g'_w is a function of Pr, M_e, g_w and a pressure gradient parameter $\overline{\beta}$, which in this case is defined by

$$\overline{\beta} = \frac{2\tilde{s}}{M_e} \frac{dM_e}{d\tilde{s}} \qquad \text{(References 2, 3, and 4)}$$

Each of the terms in equation (1) may be evaluated directly from the experimental data for surface pressure and temperature, with the exception of $(g')_w$. Evaluation of this term has been carried out by the authors of References 3, 4, and 7 for a limited number of flow conditions. In order to apply their results to the present experiments it was necessary to make interpolations which will be subsequently described.

At the forward stagnation point

$$(\dot{q})_{s=0} = \lim_{s \to 0} \dot{q} = \frac{\mu_w \rho_w}{Pr} {}^{h}s_e (g')_w \left(\frac{2 \, du_e/ds}{\rho_e \mu_e} \right) \quad (2)$$

(See Reference 2.)

The velocity du_e/ds was obtained by plotting u_e versus s from the experimental pressure data and measuring the slope.

By using equations (1) and (2) for $\dot{q}$ and the interpolated values of $(g')_w$ the theoretical curves shown in Figures 9 through 26 were obtained.

Since the assumption that Pr = 1 greatly simplifies the problem by eliminating the Mach number from the total enthalpy equation there is much more information in References 3, 4, and 7 for Pr = 1 than for the actual value Pr = 0.7 (air). Therefore, it is desirable to work out a simple relation for the effect of Prandtl number on g'_w directly from the results of the computations given in these references. For $Pr \neq 1$ one requires also the effect of Mach number on g'_w. These corrections were obtained as follows:

Step 1. Effect of Prandtl Number (M = 0)

All available information from References 3, 4, and 7 for M = 0 was plotted on a graph whose ordinate was $(-g'_w)/(g_w - g_{a_w})$ and whose abscissa was g_w. The two parameters describing these curves were $\overline{\beta}$ and Pr (Pr = 0.7 and Pr = 1.0) To discover the Prandtl number effect the value of $(-g'_w)/(g_w - g_{a_w})$ was compared for pairs of curves corresponding to the same value of $\overline{\beta}$, but two different values of Pr. For all points compared on the four related pairs of curves it was found that the values of $(-g'_w)/(g_w - g_{a_w})$ were always in the nearly-constant ratio $0.871 \pm .005$. The value .871 corresponds to $(Pr)^{.387}$ and is within 2 per cent of $(Pr)^{1/3}$ for Pr = .7. Thus

$$\left(\frac{-g'_w}{g_w - g_{a_w}} \right)_{Pr=1} \times .871 = \left(\frac{-g'_w}{g_w - g_{a_w}} \right)_{Pr=.7} .$$

By using this constant, all information given in References 3, 4, and 7 for Pr = 1 was re-evaluated at Pr = .7 and M = 0.

Step 2. Effect of Mach Number (Pr = 0.7)

In a manner similar to step 1, the results given in References 4 and 7 for Pr = .7 were plotted with an ordinate of $(-g'_w)/(g_w - g_{a_w})$ and an abscissa of

$$\frac{\frac{\gamma - 1}{2} M_e^2}{1 + \frac{\gamma - 1}{2} M_e^2} .$$

This parameter is used because it is the form in which the Mach number enters the energy equation. (See References 2 and 4.) For this plot the parameters were $\overline{\beta}$ and g_w since Pr is fixed. All of these curves were almost parallel straight lines with a slope of $.043 \pm .009$. Therefore, the Mach number

effect, although very small, was accounted for by the relation

$$\left(\frac{-g'_w}{g_w - g_{a_w}}\right)_{M=M_e} = \left(\frac{-g'_w}{g_w - g_{a_w}}\right)_{M=0} \times \left[1 + .043\left(\frac{\frac{\gamma-1}{2}M_e^2}{1+\frac{\gamma-1}{2}M_e^2}\right)\right]$$

$$= \left(\frac{-g'_w}{g_w - g_{a_w}}\right)_{M=0} \times \left[\frac{.2086 + (1/M_e^2)}{.2 + (1/M_e^2)}\right] \quad \text{for } \gamma = 1.4.$$

Step 3. Replot of $(-g'_w)/(g_w - g_{a_w})$ vs. $\overline{\beta}$ for Pr = 0.7 and M = 0

It remains only to replot the interpolated values in some convenient form, say with $(-g'_w)/(g_w - g_{a_w})$ as the ordinate and $\overline{\beta}$ as the abscissa, with g_w as the parameter. Such a plot, which was used in the calculations for Figures 9 - 26, is shown in Figure 27. In this curve Pr = .7 and M = 0. Values obtained from this plot are corrected for Mach number by the algebraic expression of step 2.

The value of the adiabatic surface enthalpy g_{a_w} for Pr = 0.7 was obtained by plotting g'_w versus g_w for a given Mach number and determining the value of g_w for which $g'_w = 0$. One finds that $g_w = 1$ for M = 0, $g_w = 0.9$ for $M = \sqrt{5}$, and $g_w = .8$ for $M = \infty$. Thus, assuming a linear dependence of g_{a_w} on the quantity

$$\frac{\frac{\gamma-1}{2}M_e^2}{1+\frac{\gamma-1}{2}M_e^2} \quad \text{one has} \quad g_{a_w} = \frac{.16 + 1/M_e^2}{.2 + 1/M_e^2}.$$

After having calculated the surface heat transfer rates with a minimum number of approximations, and compared these calculations with experimental data (Section IV), it is possible to see where additional simplifying approximations could safely be applied. According to Reference 2, the equation for heat transfer can be written as

$$\dot{q} = \sqrt{\frac{(\rho_e \mu_e)_o}{R_o}} \quad \frac{\sqrt{a^*}\ h_{s_e}}{Pr}\ g'_w\ \frac{\omega_w}{\omega_e}\ F(s)$$

where

$$F(s) = \frac{\left(\frac{p}{p_{o'}}\right)\left(\frac{\omega_e}{\omega_{e_o}}\right)\left(\frac{u_e}{a^*}\right)\left(\frac{r_o}{R_o}\right)}{\left[\int_0^{s/R_o} \left(\frac{p}{p_{o'}}\right)\left(\frac{u_e}{a^*}\right)\left(\frac{\omega_e}{\omega_{e_o}}\right)\left(\frac{r_o}{R_o}\right)^2 \frac{ds}{R_o}\right]^{\frac{1}{2}}}$$

$$\omega = \mu/RT$$

R_o = a characteristic length, say the nose radius, and

the subscript "o" means evaluation of a physical quantity at s = 0.

If we assume that ω_e/ω_{e_o} is independent of stagnation temperature, then F(s) is a function only of the pressure distribution $p/p_{o'}$ and the body shape, and need be evaluated only once for a given Mach number and body shape. In like manner if it is assumed that $\rho_e \mu_e = \rho_w \mu_w$ then $\omega_w/\omega_e = 1$ and the surface temperature distribution enters only in g_w and in the evaluation of g'_w. Therefore, with these approximations all eighteen of the heat transfer curves computed for the present experiments would have differed from each other only in the value of the quantity $\sqrt{(\rho_e \mu_e)_o}\ \sqrt{a^*}\ h_{s_e}\ g'_w$. This simplification obviously constitutes a tremendous saving in labor with a small sacrifice in accuracy.

IV. DISCUSSION OF RESULTS

In Figures 9 - 26 the theoretical curves (Section III) are compared with the appropriate experimental heat transfer data. The surface temperature distribution is obtained by averaging the experimental points, but in the heat transfer plots the actual experimental data is shown. In both the surface temperature and heat transfer plots, the abscissa is the distance in inches from the stagnation point of the model measured along the model surface.

In general the agreement between theory and experiment is very satisfactory over the forward portion of the body. Therefore it is believed that these heat meters have proved themselves as heat transfer measuring devices. The only point of significant disagreement is on the aft section of the body where the experimental data is twice the value of the theoretical value in some cases. This discrepancy is perhaps due to faulty calibration at the low output values. There may also be a small correction to the theory (of the order of 10 per cent) because of our assumption of local similarity. It is also possible that this difference is caused in part by radiation from the tunnel walls. (See Appendix B.) There is little radiative heat transfer for the air-cooled model because of its high surface temperature, and the curves show a very small error on the aft part of this model.

Future work with these meters could include application to any body shape for which a calibration oven could be built. Much information could be obtained using these meters on models with film or porous cooling. An improvement in design might be made by installing the meters in small plugs which could be individually calibrated before

installation in a model. By this means a much simpler and probably more accurate calibration oven could be used.

REFERENCES

1. DeLauer, R. D. and Nagamatsu, H. T.: Experimental Heat Transfer at Hypersonic Mach Number. GALCIT Memorandum No. 14, April 15, 1953.

2. Lees, L.: Laminar Heat Transfer over Blunt-Nosed Bodies at Hypersonic Flight Speeds. Jet Propulsion, Vol. 26, No. 4, pp. 259-269, April, 1956.

3. Cohen, C. B. and Reshotko, E.: Similar Solutions for the Compressible Laminar Boundary Layer with Heat Transfer and Pressure Gradient. NACA TN 3325, February, 1955.

4. Levy, S.: Effect of Large Temperature Change (Including Viscous Heating) upon Laminar Boundary Layers with Variable Free-Stream Velocity. Journal of the Aeronautical Sciences, Vol. 21, No. 7, pp. 459-474, July, 1954.

5. Crawford, D. H. and McCauley, W. D.: Investigation of the Laminar Aerodynamic Heat-Transfer Characteristics of a Hemisphere-Cylinder in the Langley 11-Inch Hypersonic Tunnel at a Mach Number of 6.5. NACA TN 3706, July, 1956.

6. Schmidt, C. M. and Hanawalt, A. J.: The Effect of an Arbitrary Distribution of Surface Temperature on Heat Transfer in the Compressible Boundary Layer. Journal of the Aeronautical Sciences, Vol. 24, No. 1, pp. 73-74, January, 1957.

7. Reshotko, E. and Cohen, C. B.: Note on the Compressible Laminar Boundary Layer with Heat Transfer and Pressure Gradient. Journal of the Aeronautical Sciences, Vol. 22, No. 8, pp. 584-585, August, 1955.

8. Bureau of Ordnance: Handbook of Supersonic Aerodynamics. NAVORD Report 1488, (Vol. 5), August, 1953.

9. Ames Aeronautical Laboratory Research Staff: Equations, Tables, and Charts for Compressible Flow. NACA Technical Report 1135, 1953.

10. McAdams, W. H.: Heat Transmission. McGraw-Hill, New York, 1954.

11. Hartwig, F. W., Bartsch, C. A., and McDonald, H.: Miniaturized Heat Meter for Steady State Aerodynamic Heat Transfer Measurements. Journal of the Aeronautical Sciences, Vol. 24, No. 3, pp. 239, March, 1957.

12. Eimer, M. and Nagamatsu, H. T.: Direct Measurement of Laminar Skin Friction at Hypersonic Speeds. GALCIT Memorandum No. 16, July, 1953.

13. Baloga, P. E. and Nagamatsu, H. T.: Instrumentation of GALCIT Hypersonic Wind Tunnels. GALCIT Memorandum No. 29, July, 1955.

APPENDIX A

HEAT METER CONSTRUCTION

A sheet of microscopic slide glass approximately .5" x .5" x .007" was coated with wax. Then lines were scribed through the wax .062" apart. The glass was immersed in hydrofluoric acid which cut the glass along the scribed lines into strips .5" x .062" x .007". The wax was removed, and the strip was then ready for winding. A special lathe was built with chucks which held the glass ends. The two chucks were geared together so as to prevent any relative movement and thus avoid torsional stresses in the glass. The glass was wrapped with two .001" constantan wires at once. The second wire, acting as a spacer for the first wire, was removed, leaving a uniformly spaced winding. A normal meter had 50 turns of wire. (See Figure 3.) After proper masking, one half of each loop was silver-plated by placing the edge of the meter half way into a silver plating solution. Each meter was given a protective coat of cement to avoid damage and prevent unwinding of the wires. Finally the excess glass on the ends was broken off leaving a meter 1/8" x 1/16" x 1/100". (See Figure 4.) For a further discussion see Reference 11.

APPENDIX B

SAMPLE RADIATION CALCULATION

Consider the case p_o = 300 psig and T_o = 700°F with tunnel wall temperature = 320°F for the water-cooled metal model. On the cylindrical part of the model the surface temperature was approximately 90°F.

From Reference 10, page 78, eq. (4.37)

$$\dot{q}_{rad.} = \sigma \left[\varepsilon_1 T_1^{\,4} - a_{12} T_2^{\,4}\right] = \text{radiant heat transfer}$$

where

σ = .1713 x 10^{-8} BTU/ft.^{2}/hr./°R

ε_1 = approximately .90 = a_{12}

T_1 = 320°F

T_2 = 90°F

$$\therefore \dot{q}_{rad.} = .1713 \times .90 \left[\left(\frac{460 + 320}{100}\right)^4 - \left(\frac{460 + 90}{100}\right)^4\right]$$

$$= 440 \text{ BTU/ft.}^2\text{/hr.}$$

Since ε_1 and a_{12} are somewhat indefinite this correction was not applied. It is shown merely to demonstrate the order of magnitude of the correction. The difference between theory and experiment for this point is about 1000 BTU/ft.^{2}/hr., which indicates that radiation is a large contributing factor.

(a)

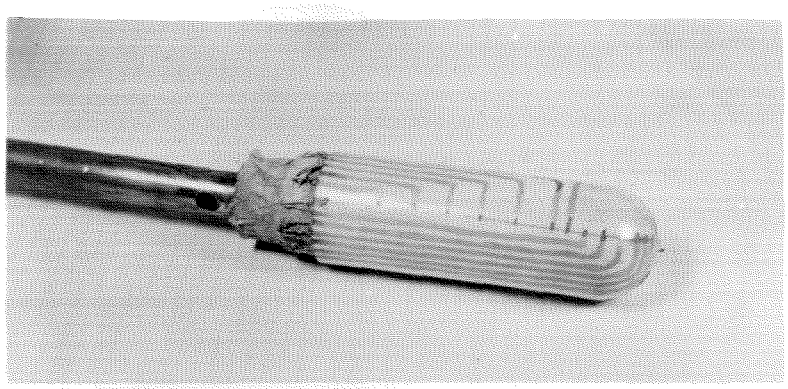

(b)

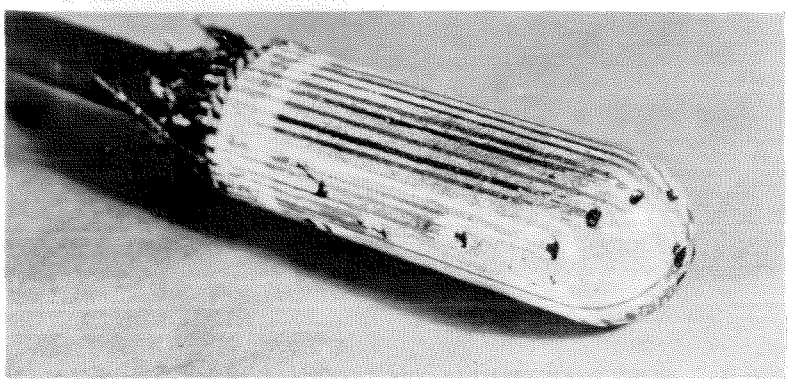

FIG. 1(a) - MODEL SHOWING THERMOCOUPLES
(b) - MODEL SHOWING HEAT METERS

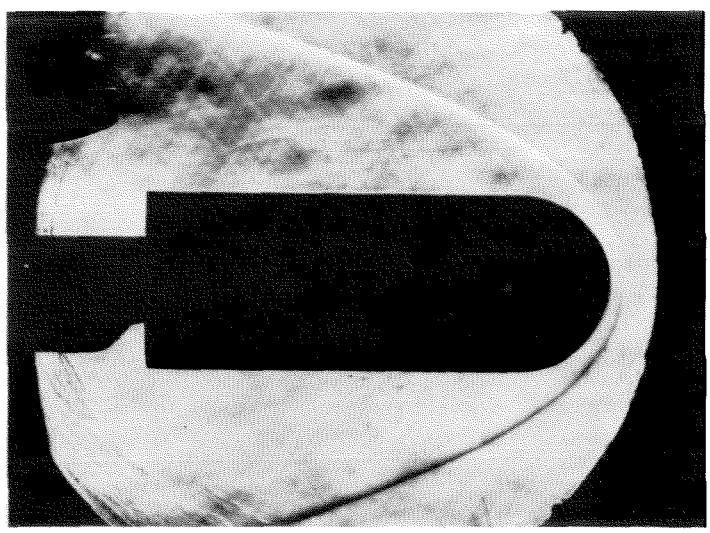

FIG. 2 - SCHLIEREN PICTURE OF MODEL AND SHOCK WAVE

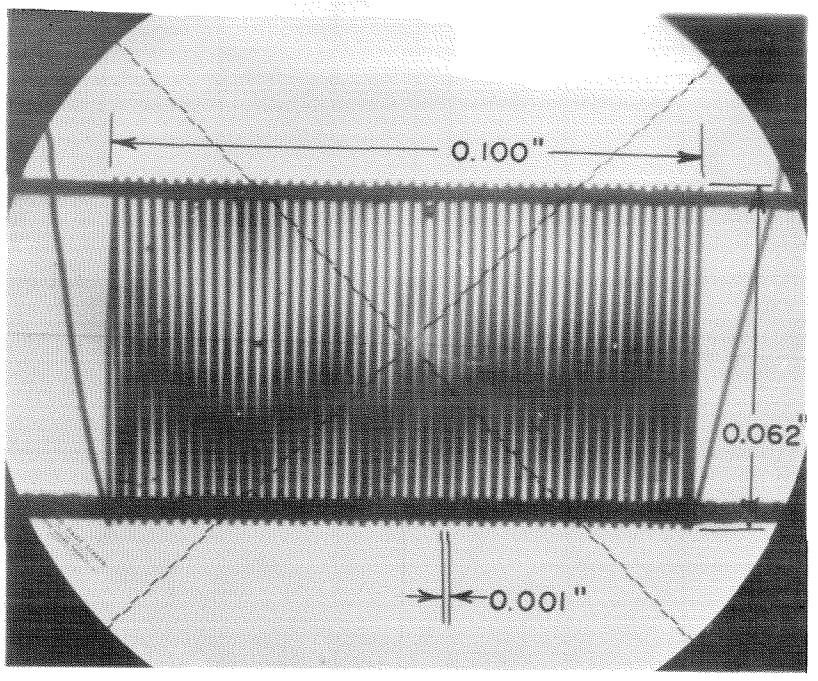

FIG. 3 - VIEW THROUGH A HEAT METER AS SEEN ON A CONTOUR PROJECTOR

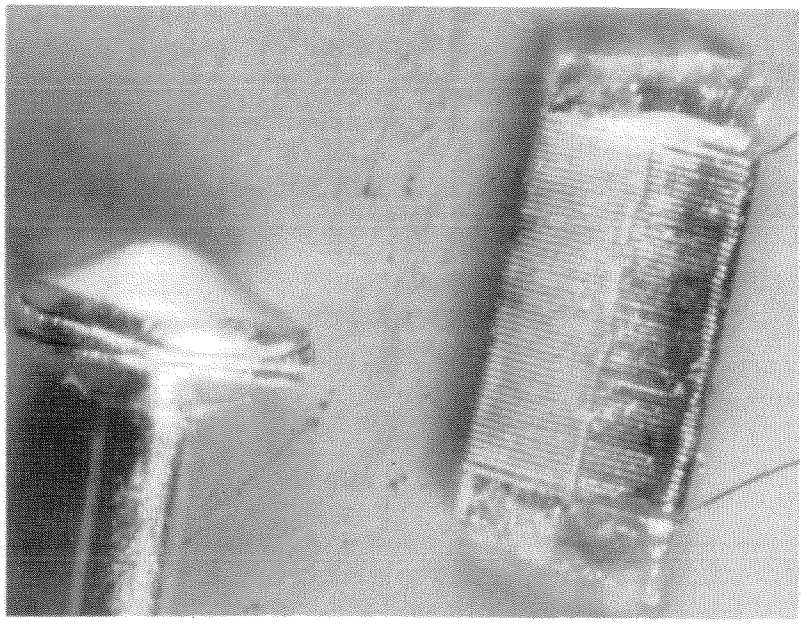

FIG. 4 - HEAT METER COMPARED TO ORDINARY PINHEAD

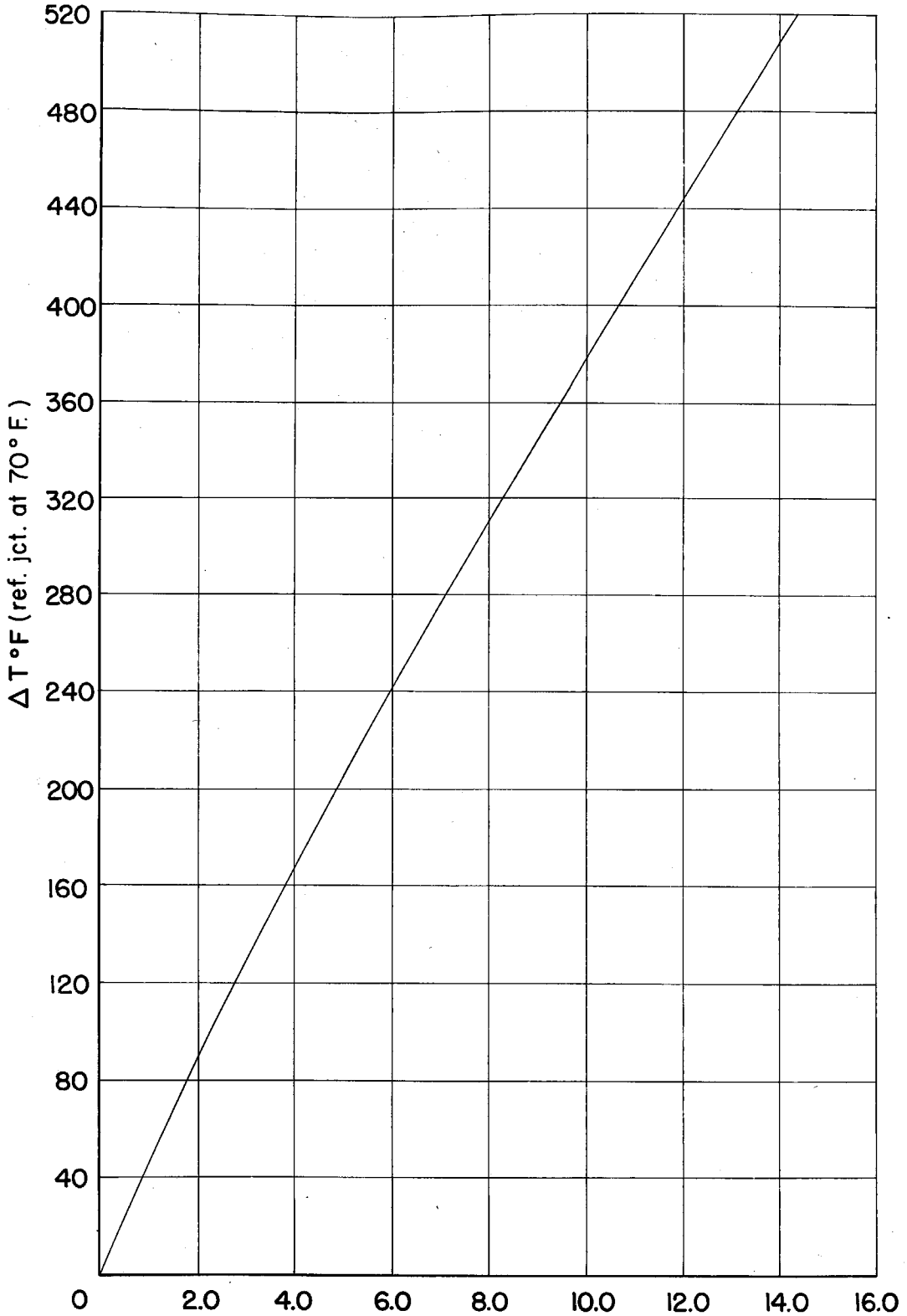

Fig. 5

SILVER CONSTANTAN THERMOCOUPLE CALIBRATION

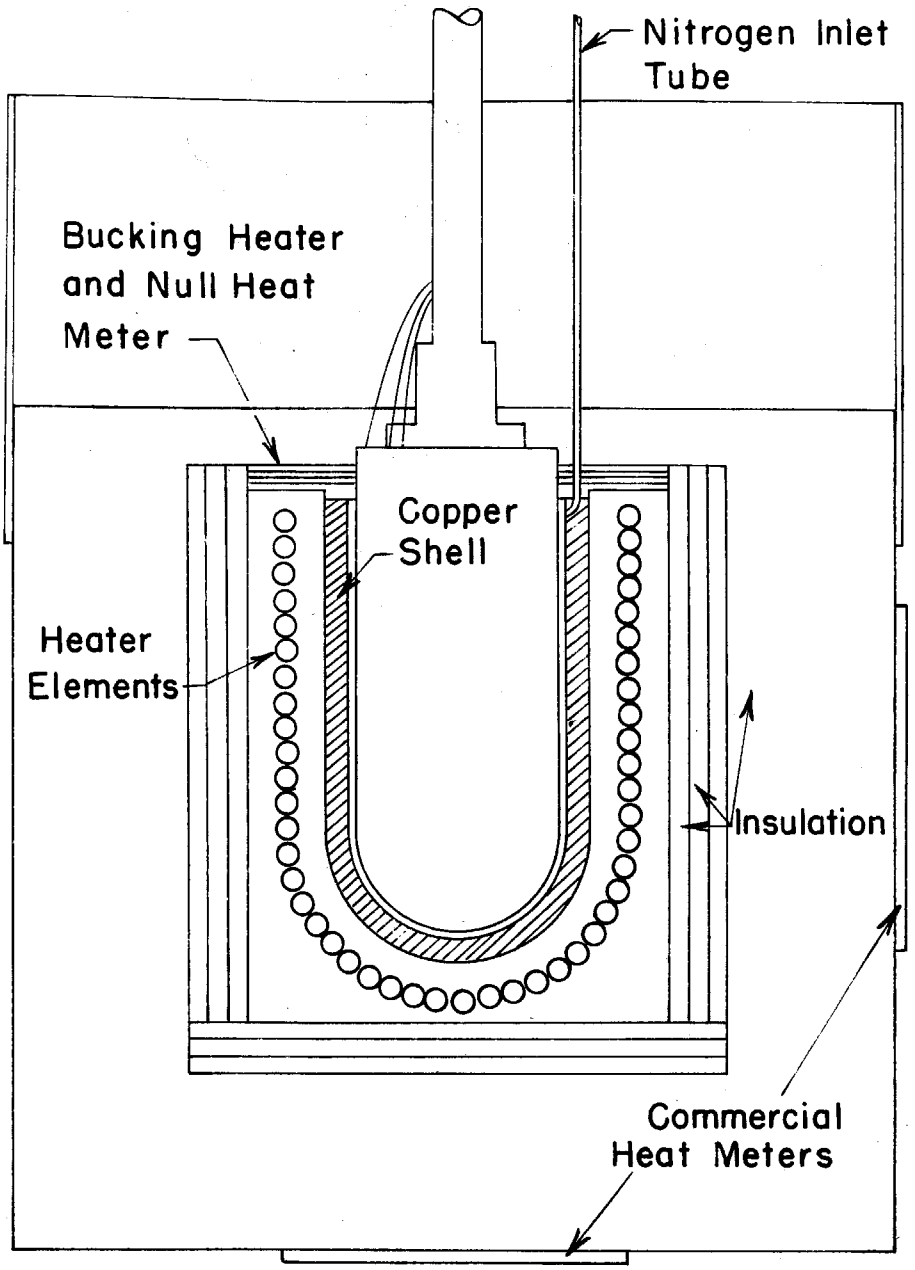

CALIBRATION OVEN - CROSS SECTION

Fig. 6

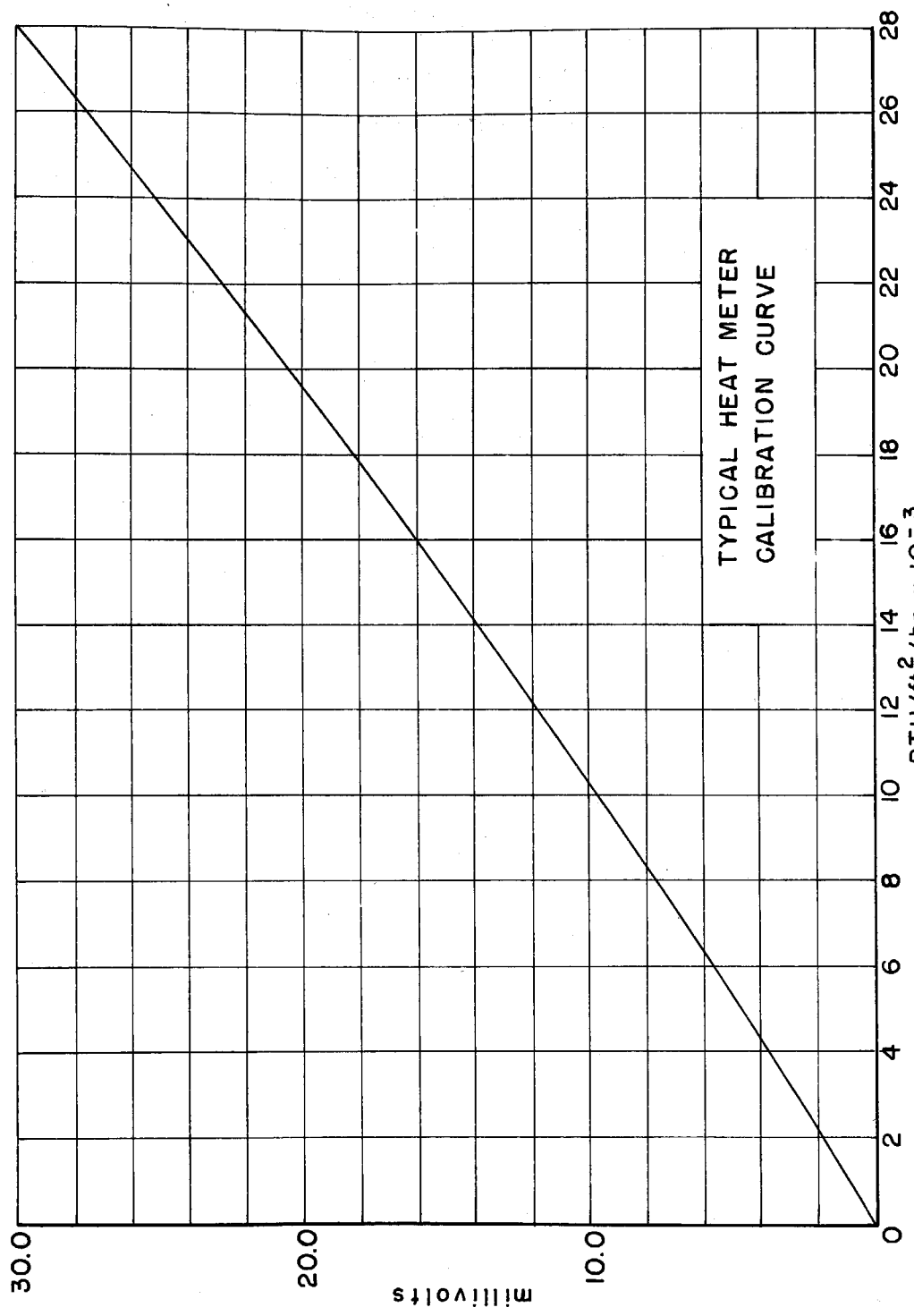
TYPICAL HEAT METER
CALIBRATION CURVE
millivolts
30.0
20.0
10.0
0
2
4
6
8
10
12
14
16
18
20
22
24
26
28
BTU/ft.²/hr. x 10⁻³

Fig. 7

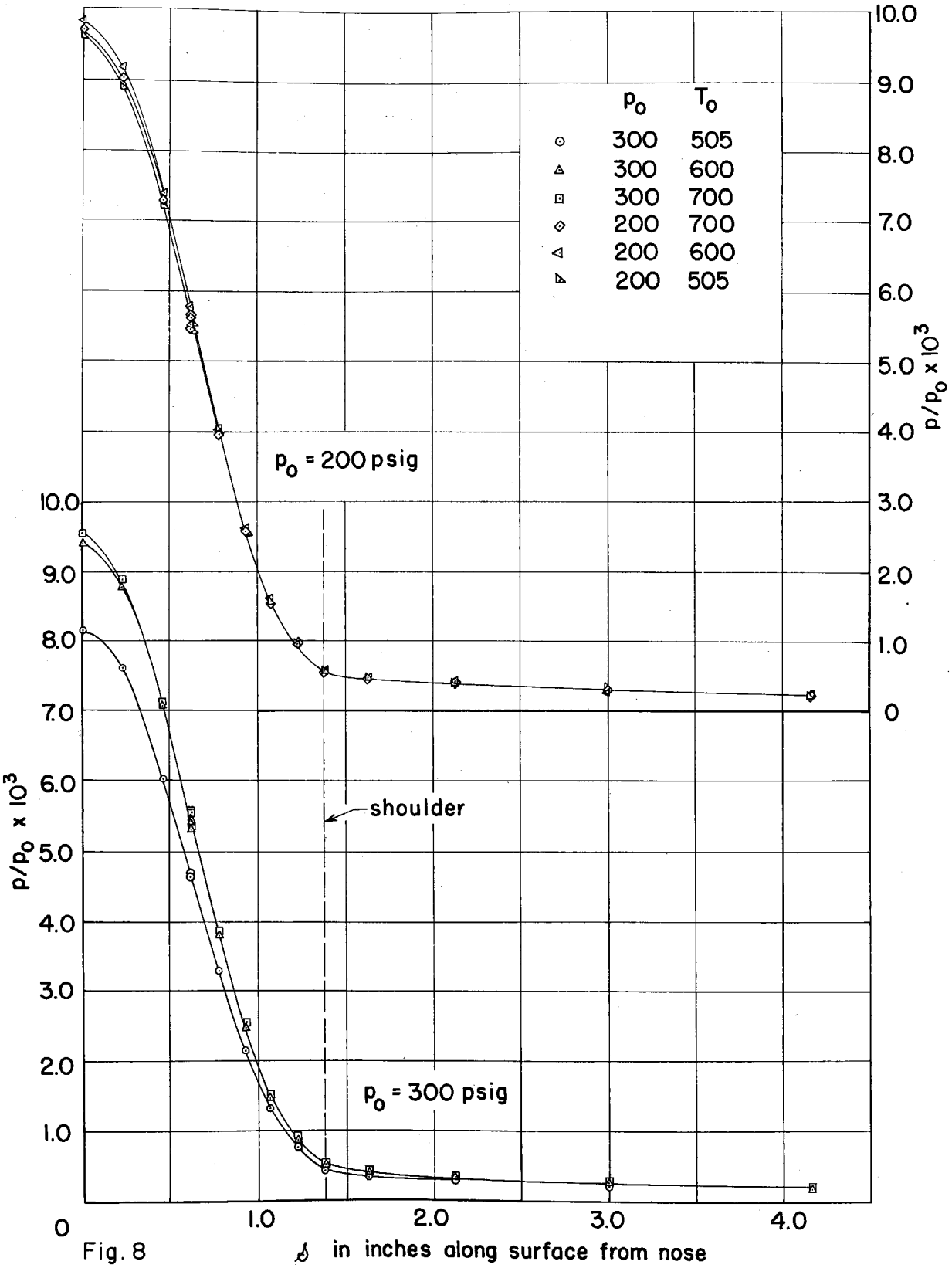

Fig. 8 PRESSURE DISTRIBUTION

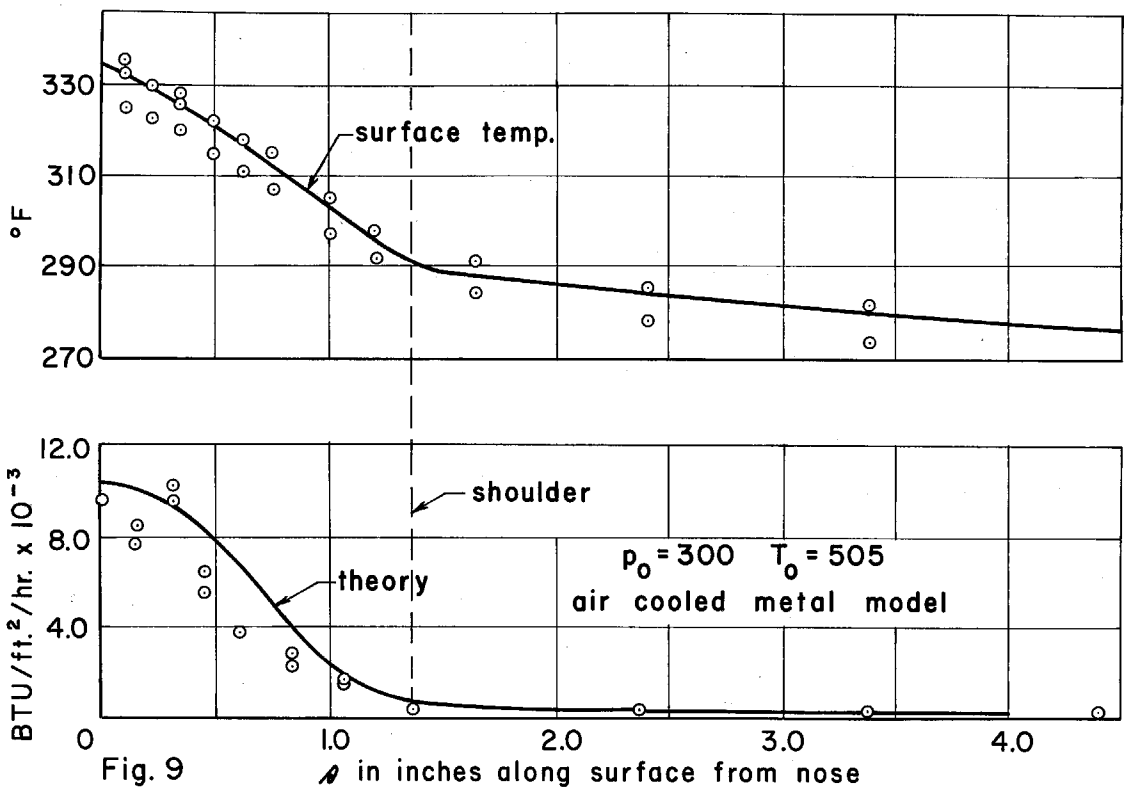

Fig. 9

TEMP. AND HEAT TRANSFER DISTRIBUTION

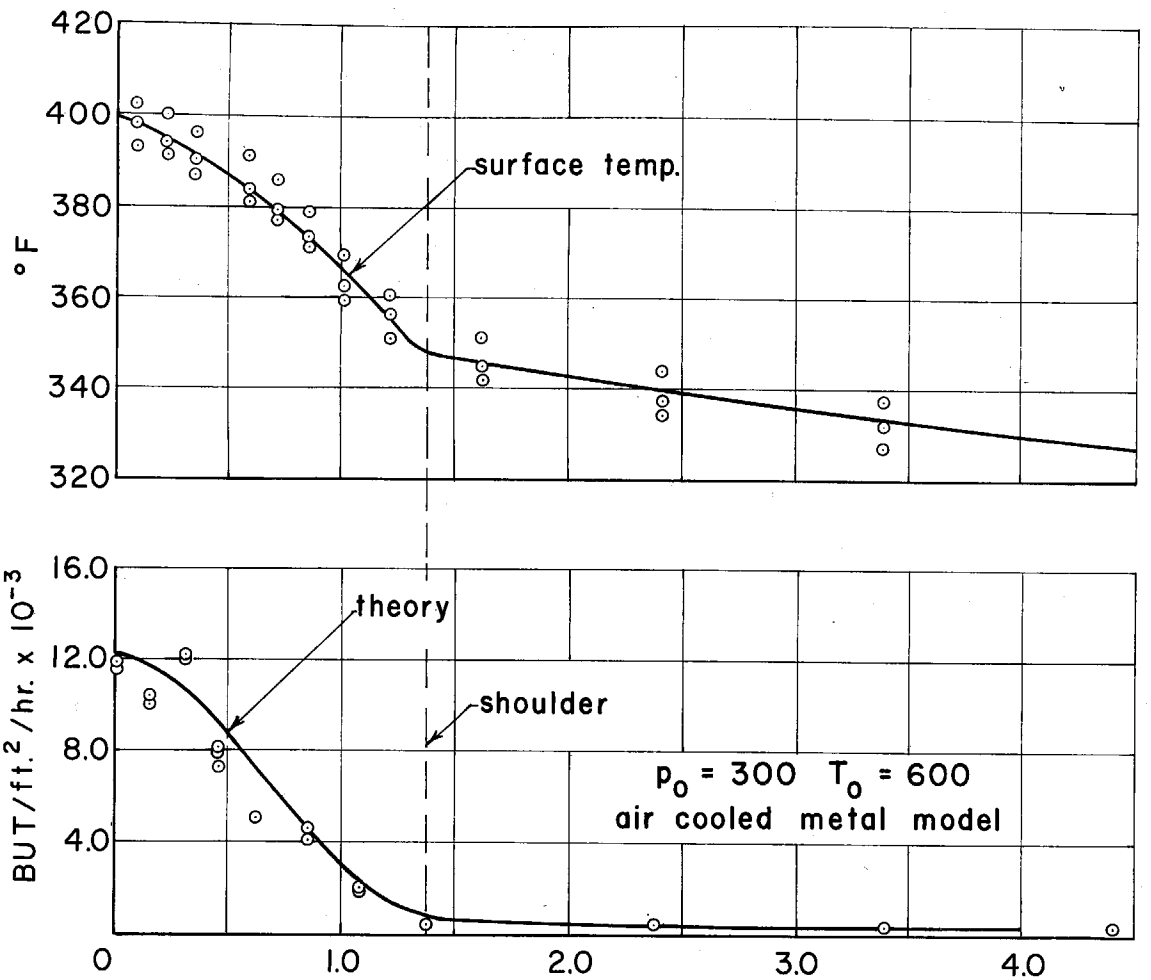

Fig. 10

TEMP. AND HEAT TRANSFER DISTRIBUTION

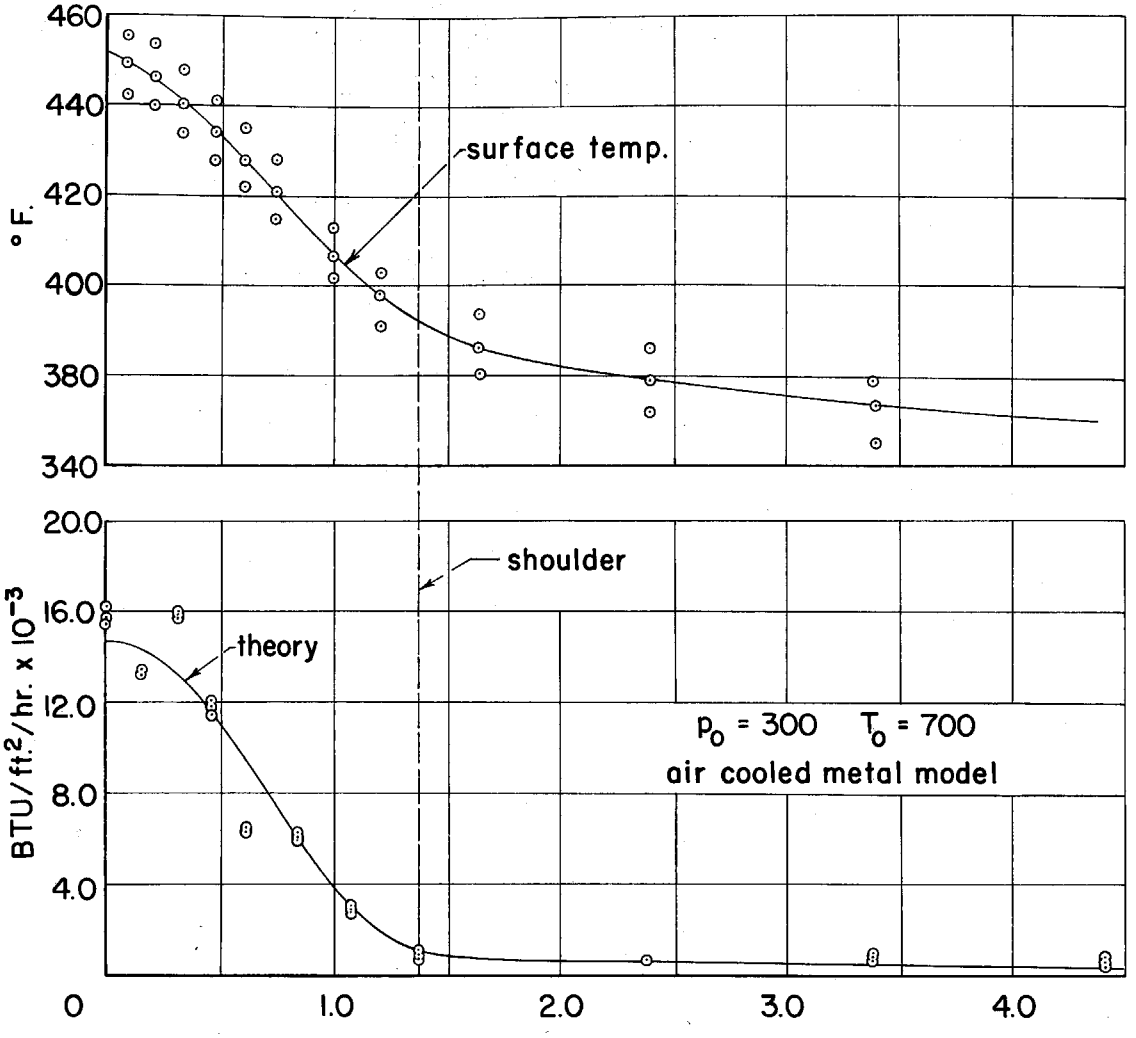

Fig. 11

TEMP. AND HEAT TRANSFER DISTRIBUTION

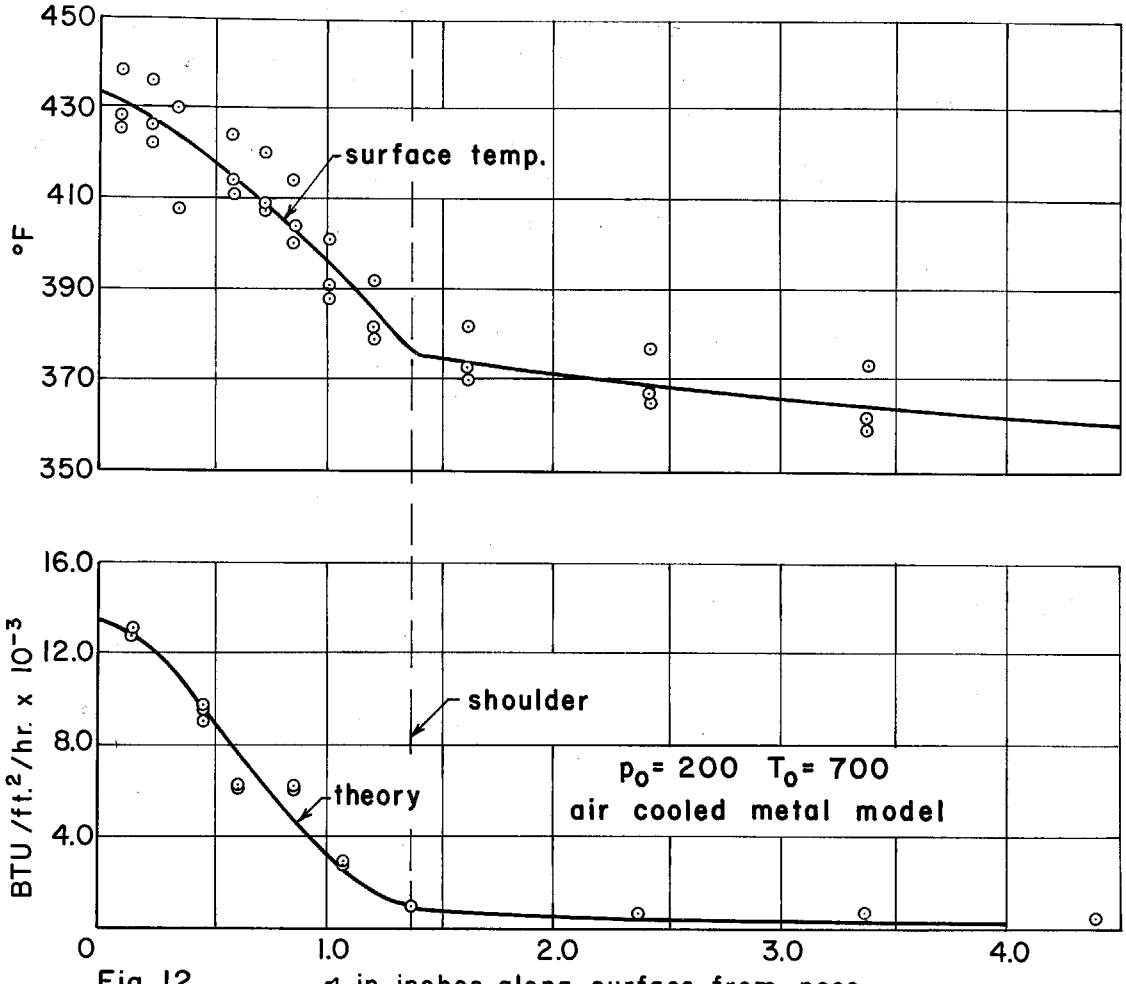

Fig. 12

TEMP. AND HEAT TRANSFER DISTRIBUTION

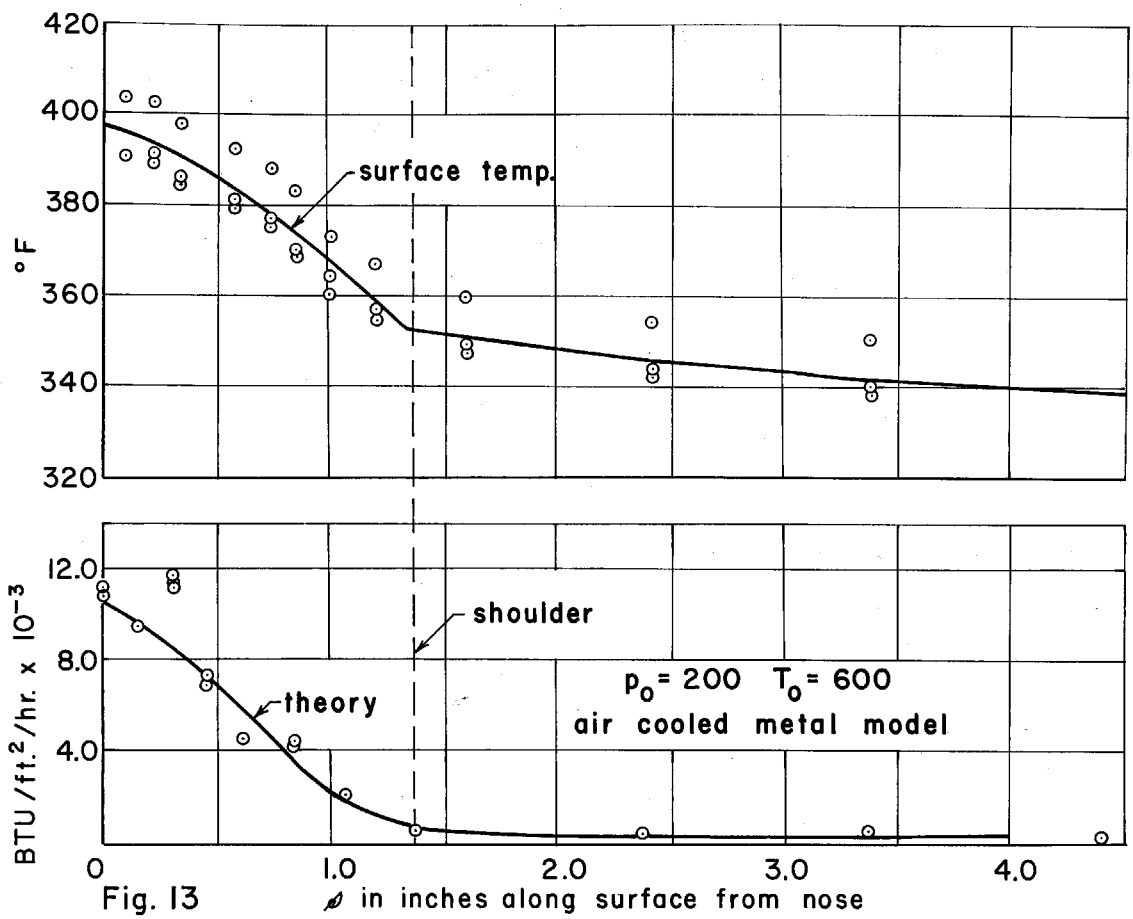

Fig. 13 TEMP. AND HEAT TRANSFER DISTRIBUTION

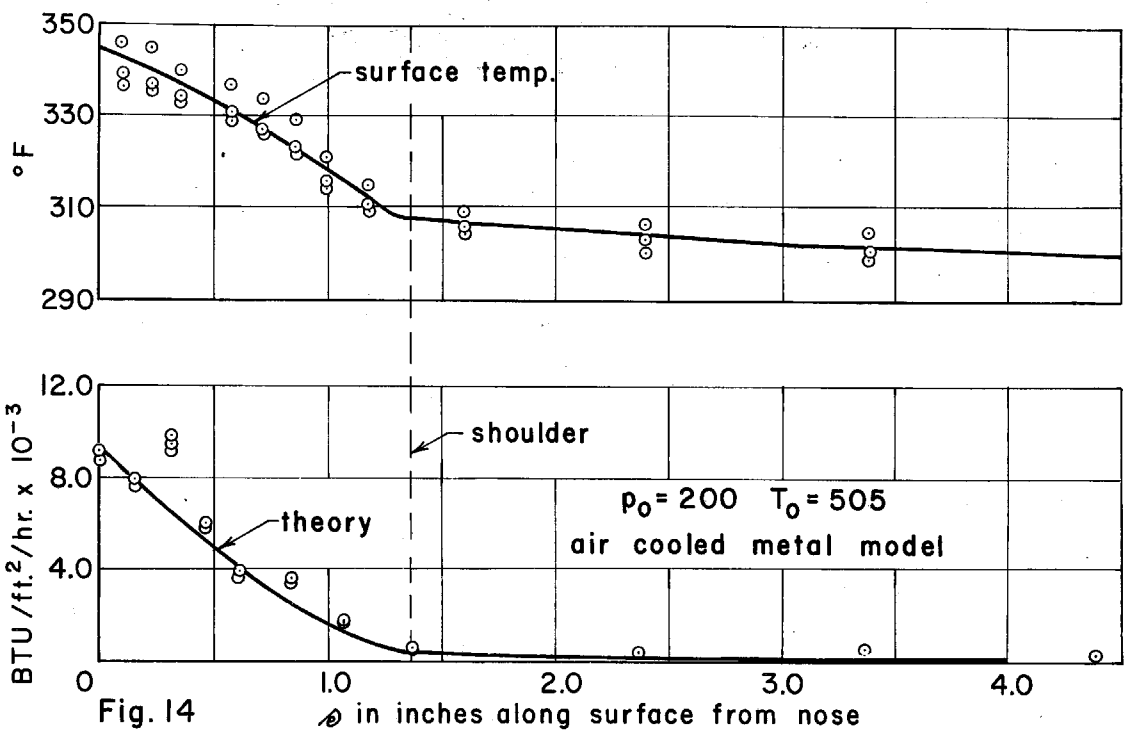

Fig. 14

TEMP. AND HEAT TRANSFER DISTRIBUTION

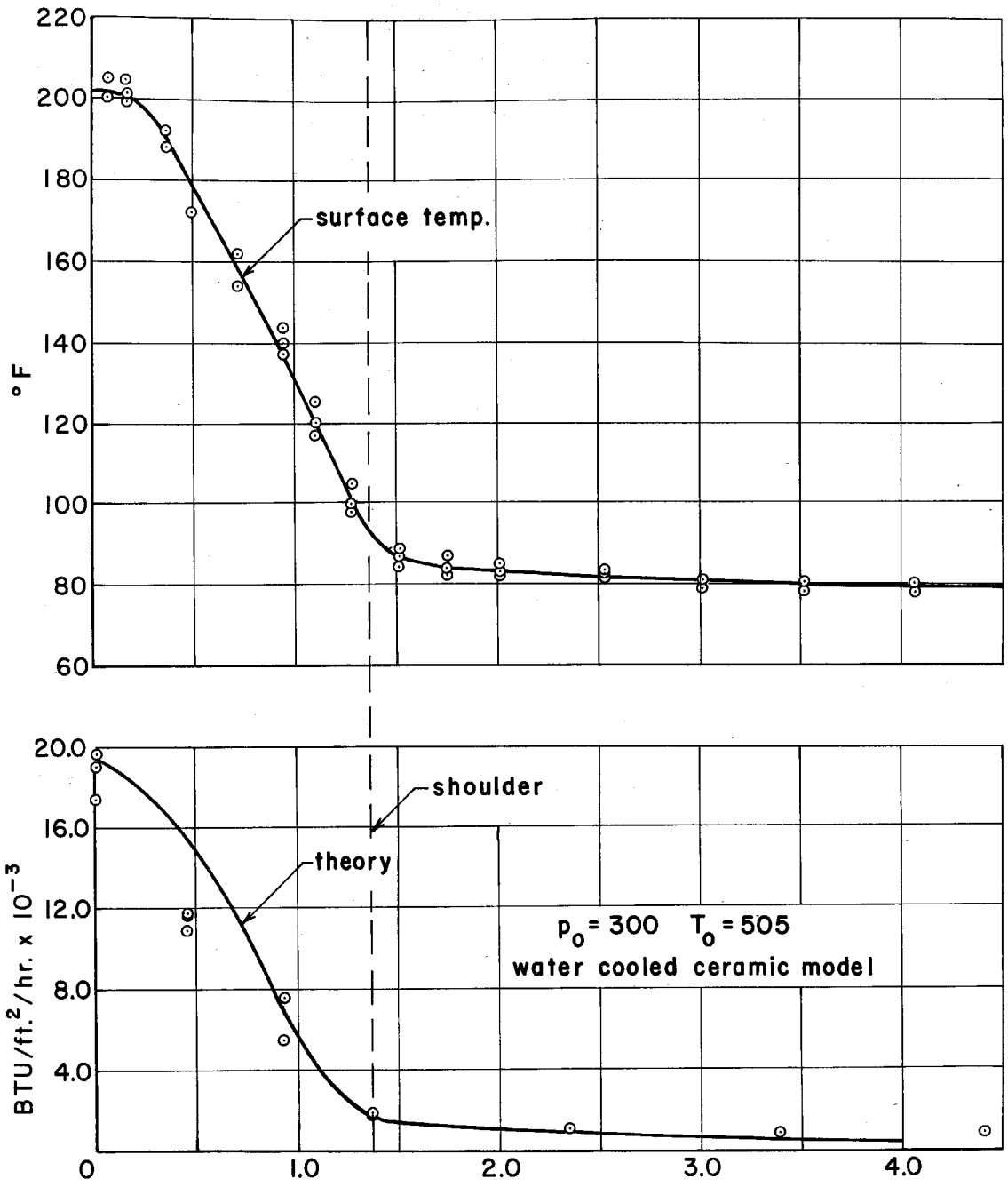

Fig. 15 TEMP. AND HEAT TRANSFER DISTRIBUTION

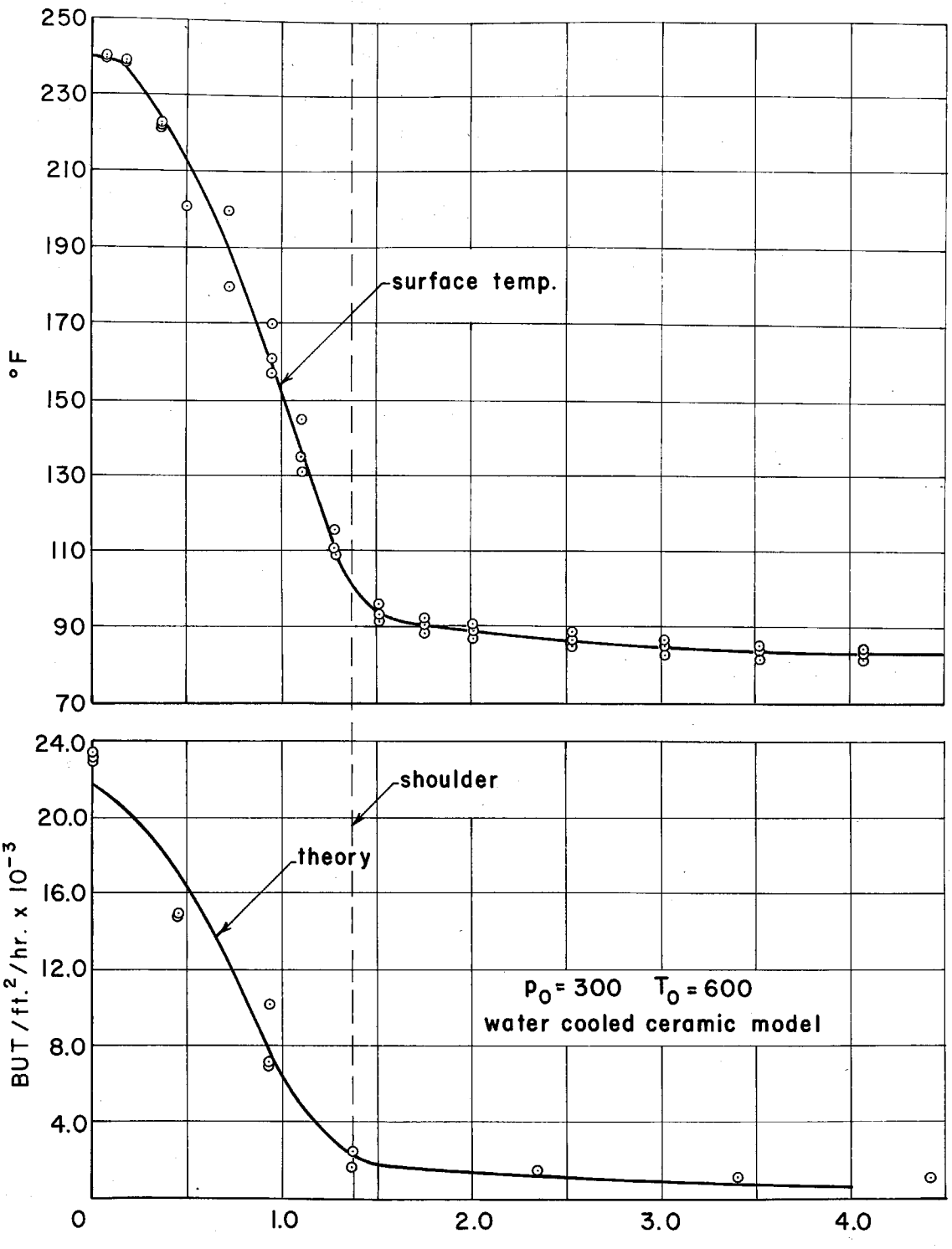

Fig. 16

TEMP. AND HEAT TRANSFER DISTRIBUTION

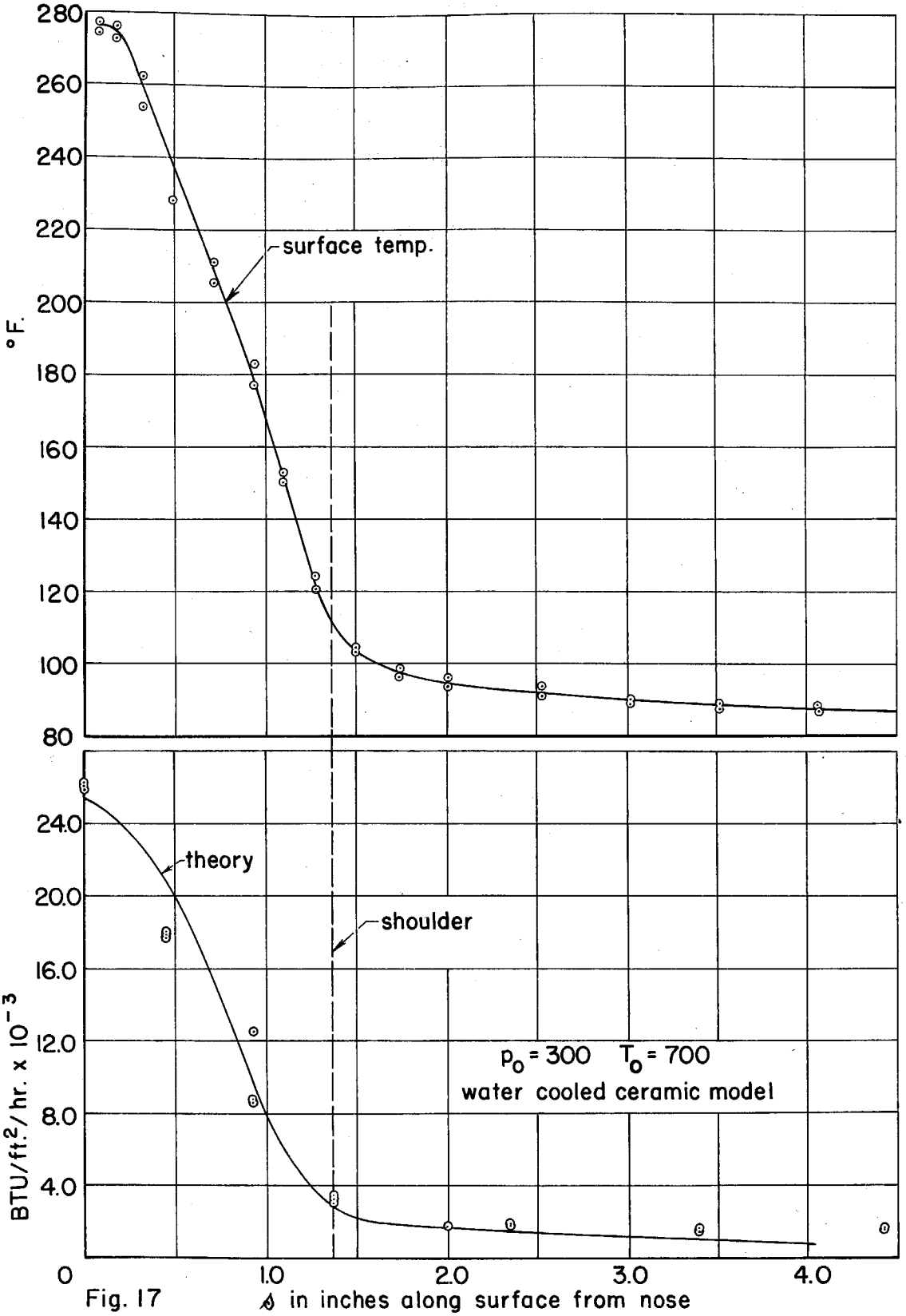

Fig. 17 TEMP. AND HEAT TRANSFER DISTRIBUTION

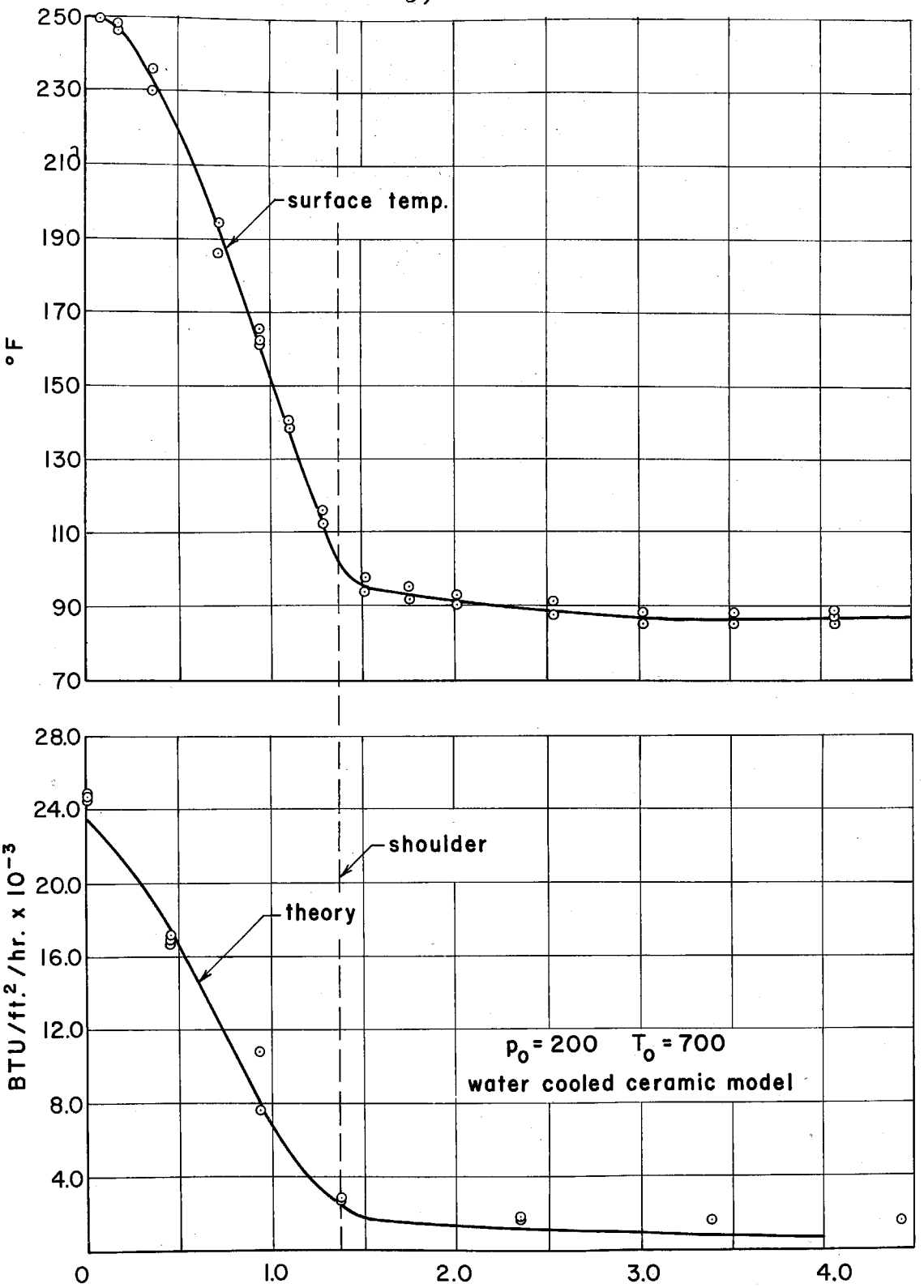

Fig. 18

TEMP. AND HEAT TRANSFER DISTRIBUTION

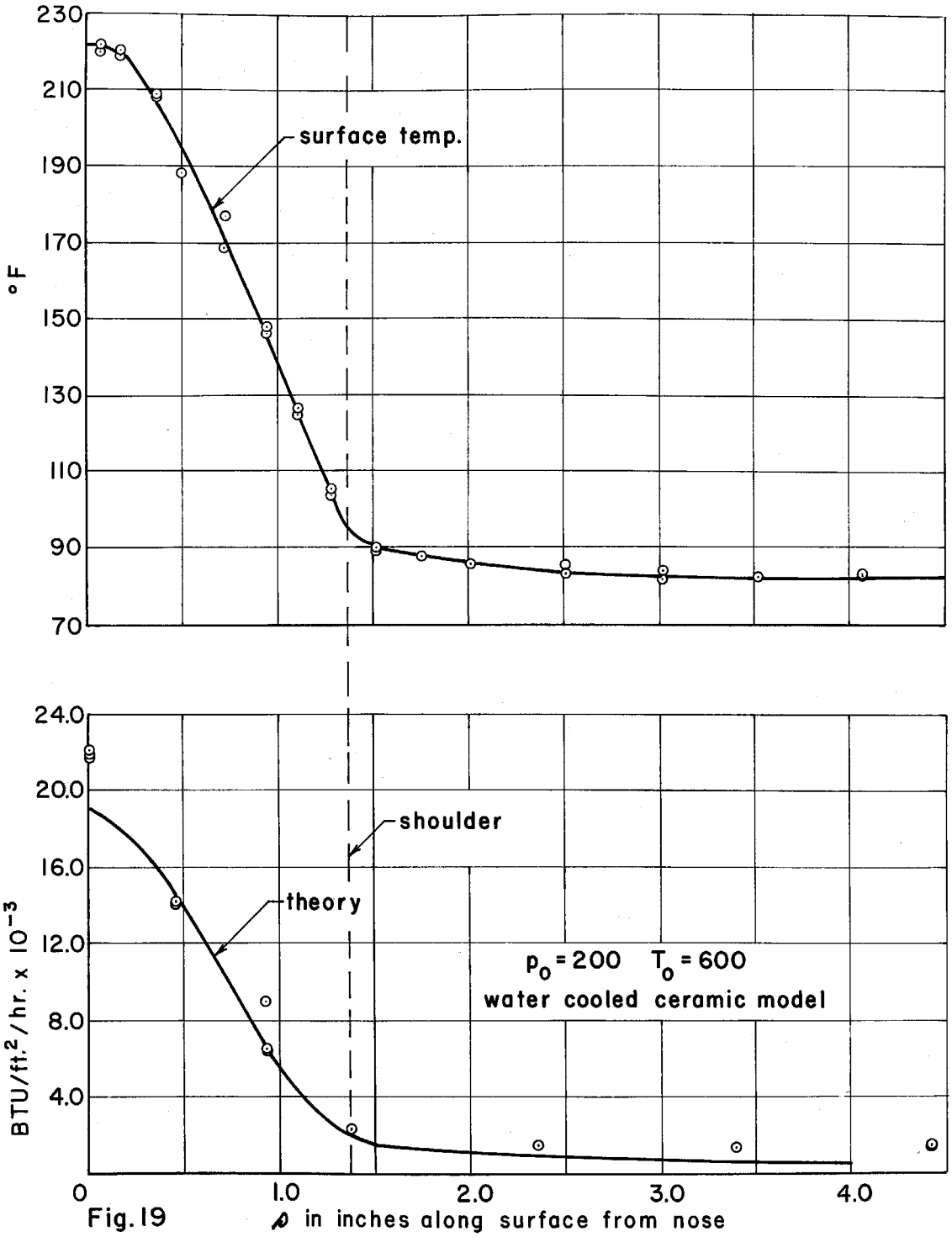

Fig. 19 TEMP. AND HEAT TRANSFER DISTRIBUTION

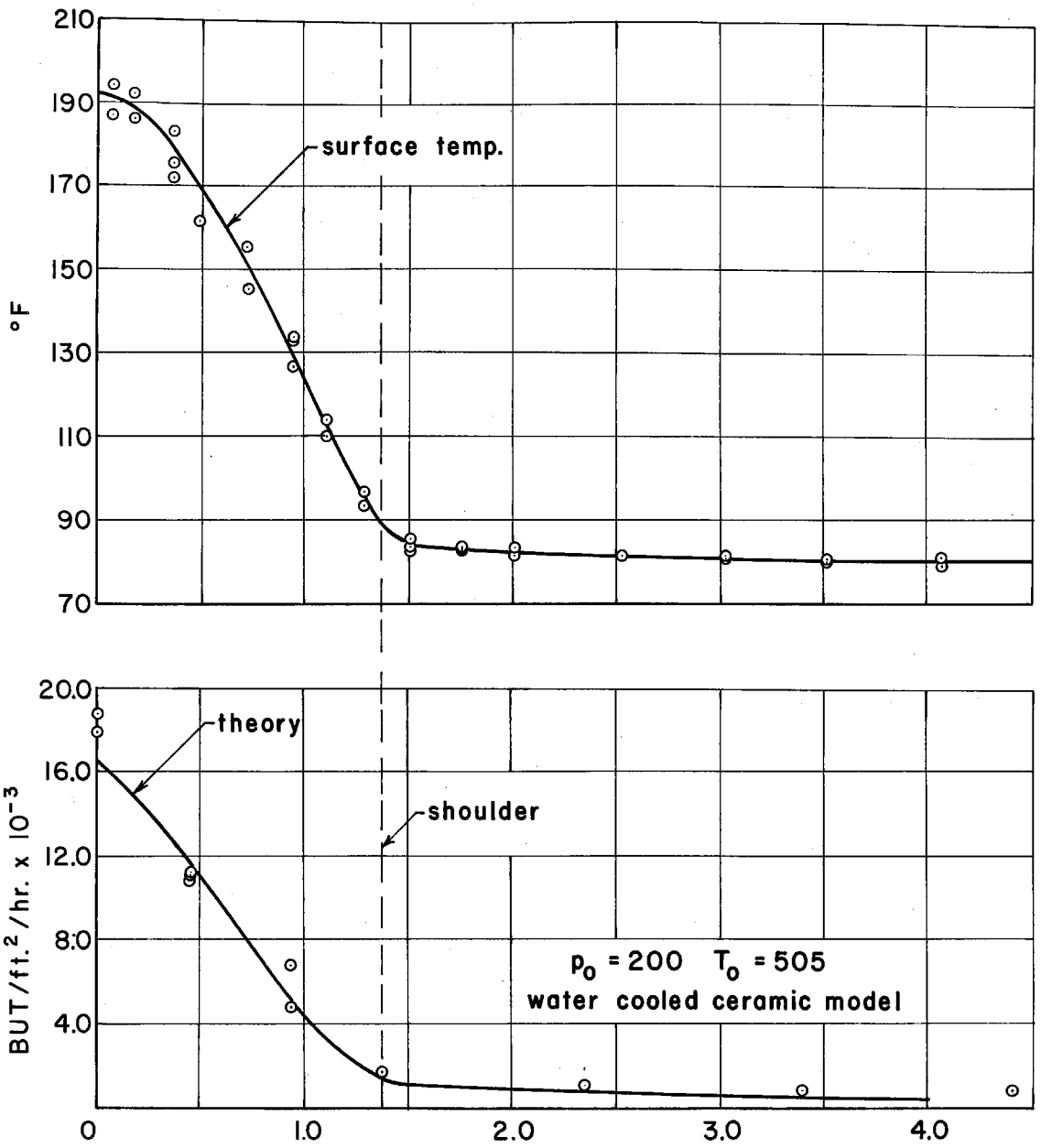

Fig. 20

TEMP. AND HEAT TRANSFER DISTRIBUTION

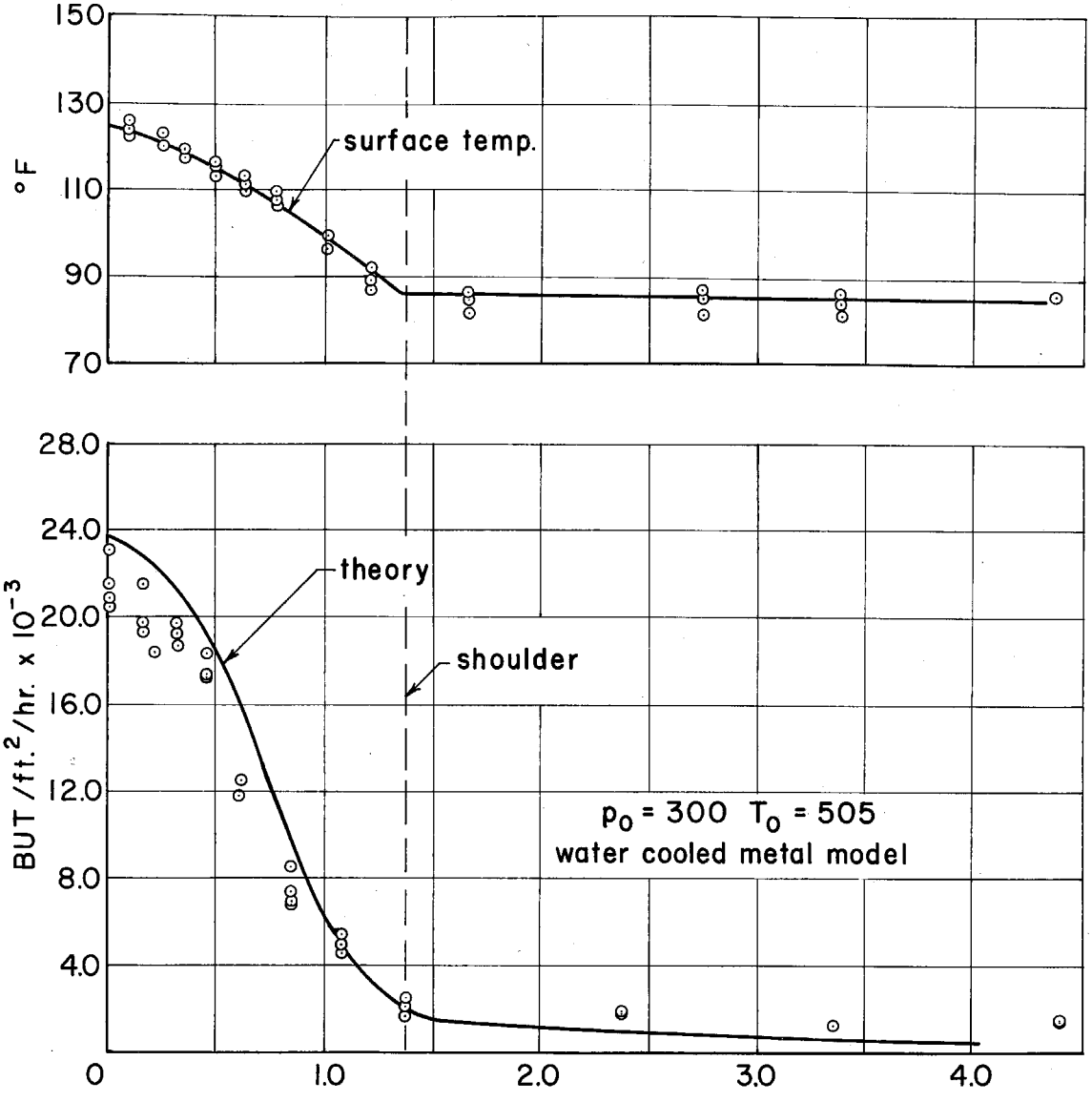

Fig. 21

TEMP. AND HEAT TRANSFER DISTRIBUTION

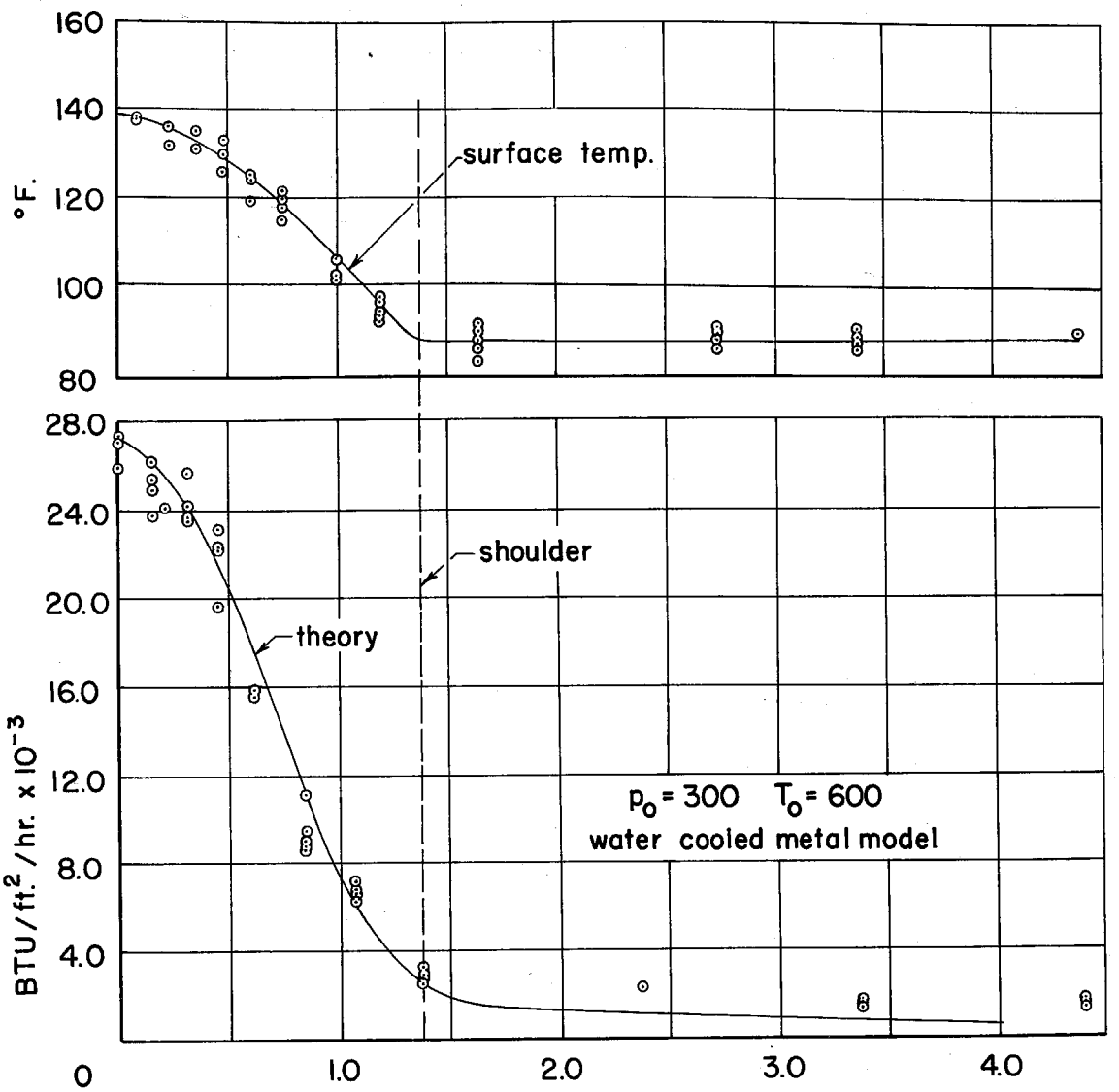

Fig. 22 δ in inches along surface from nose

TEMP. AND HEAT TRANSFER DISTRIBUTION

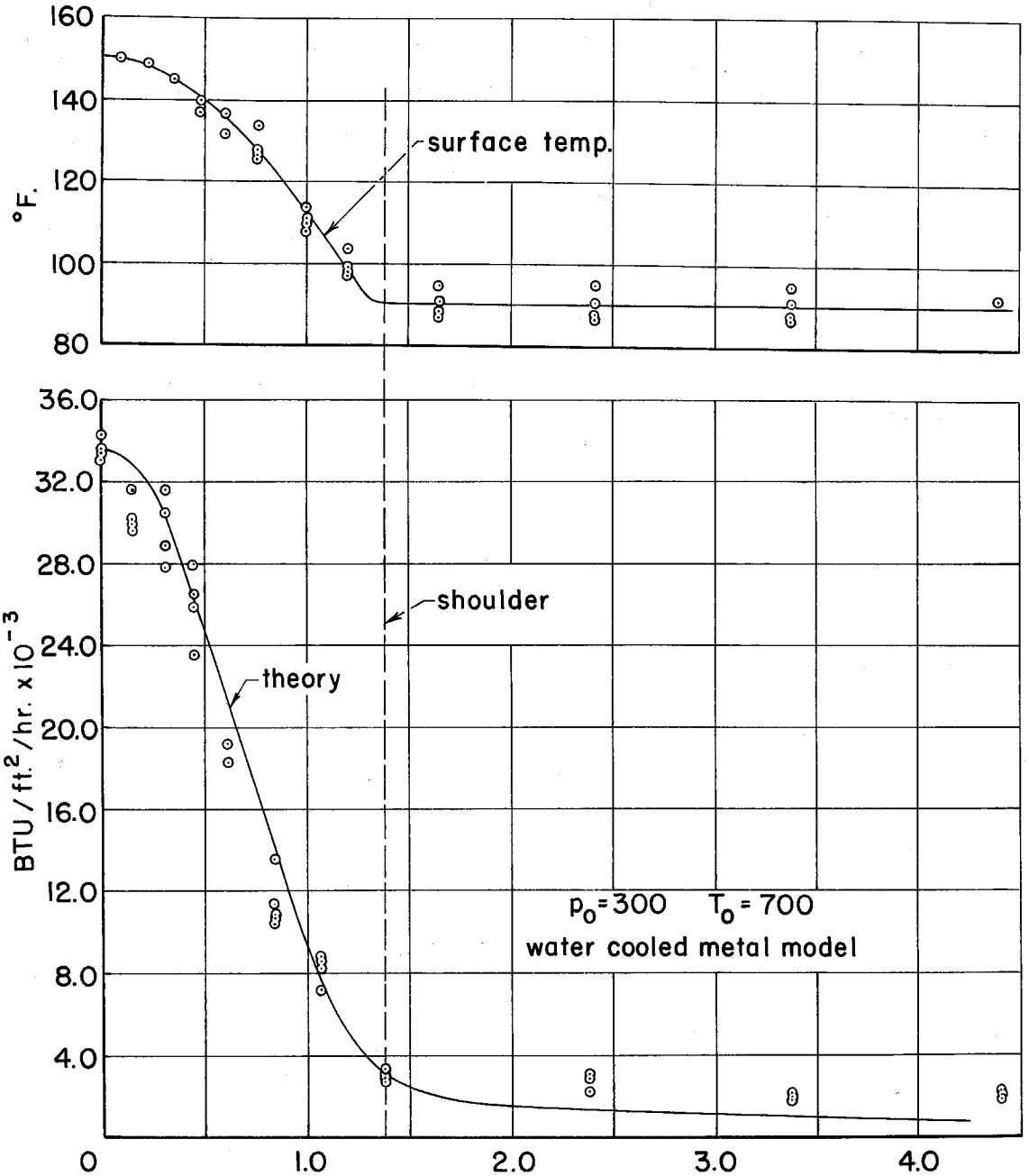

Fig. 23 ϕ in inches along surface from nose

TEMP. AND HEAT TRANSFER DISTRIBUTION

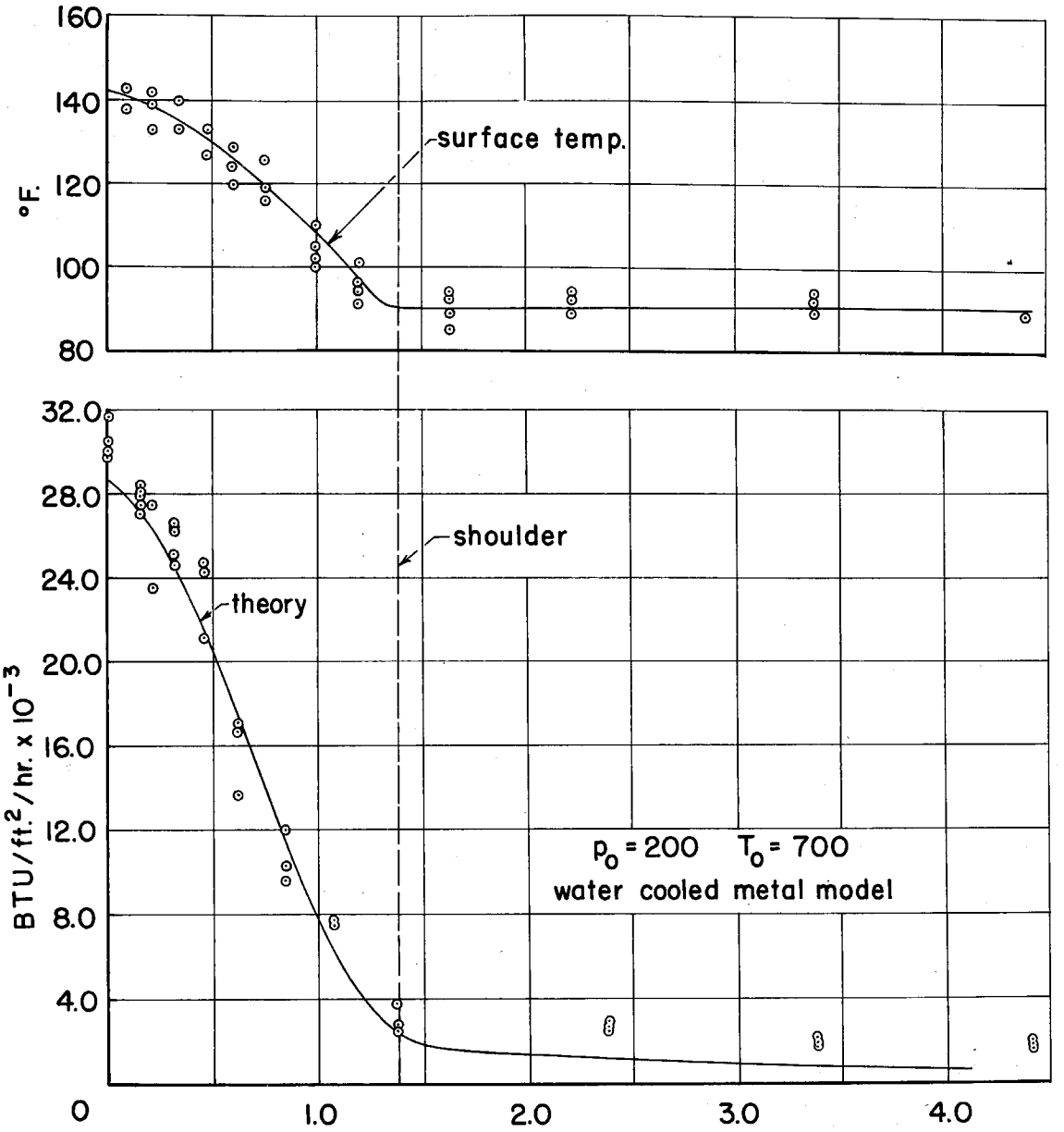

Fig. 24 δ in inches along surface from nose

TEMP. AND HEAT TRANSFER DISTRIBUTION

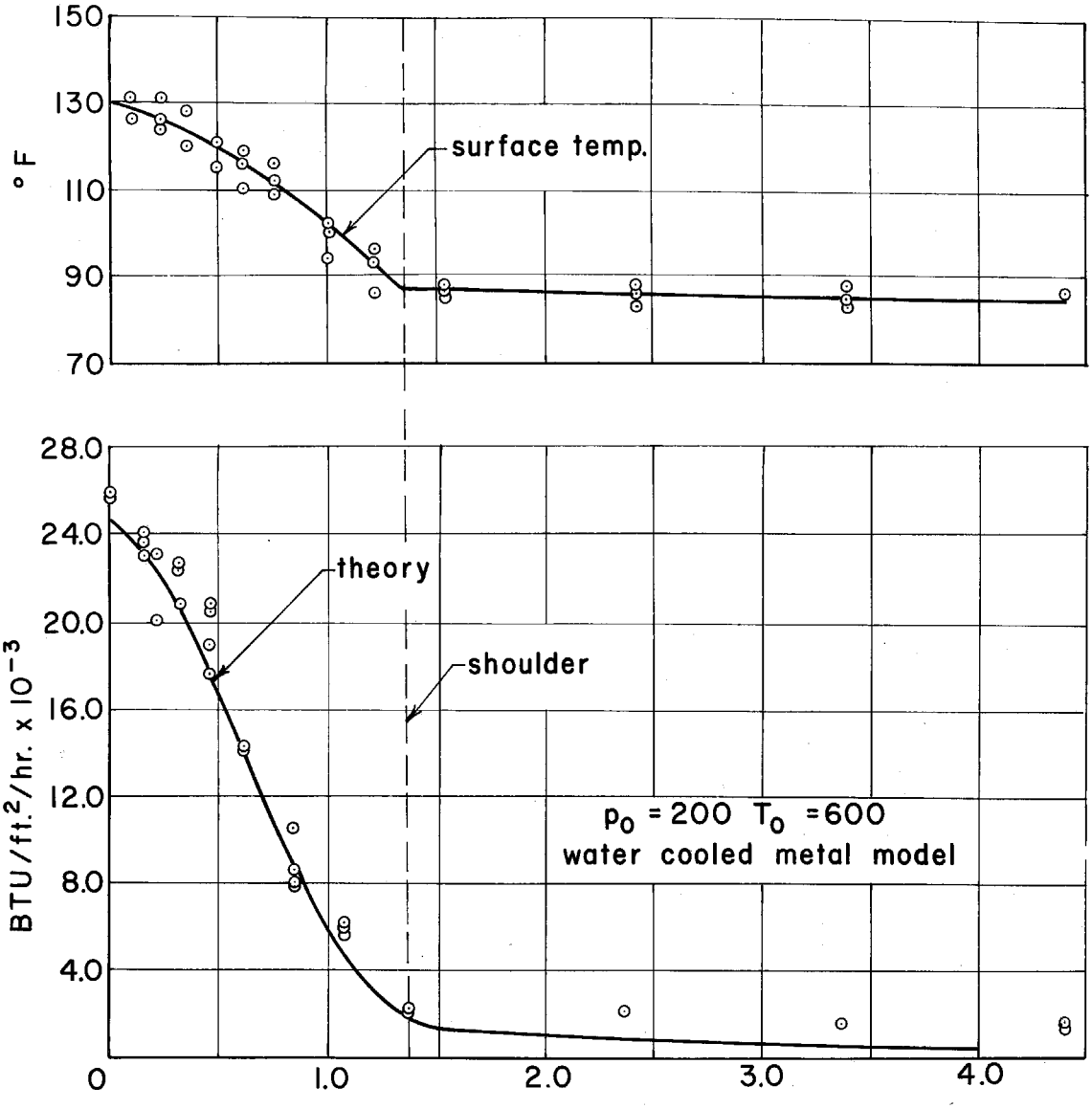

Fig. 25

TEMP. AND HEAT TRANSFER DISTRIBUTION

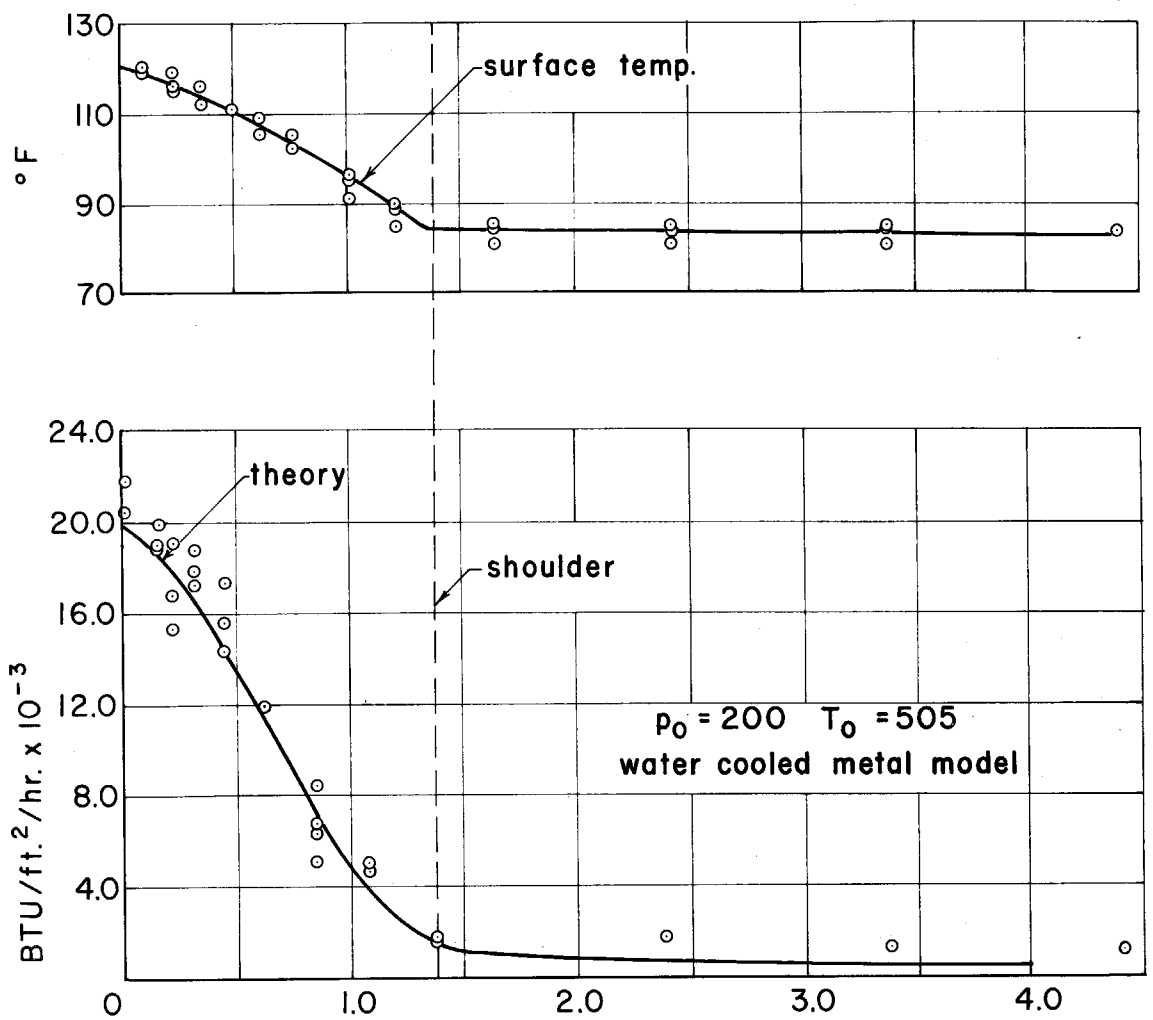

Fig. 26

TEMP. AND HEAT TRANSFER DISTRIBUTION

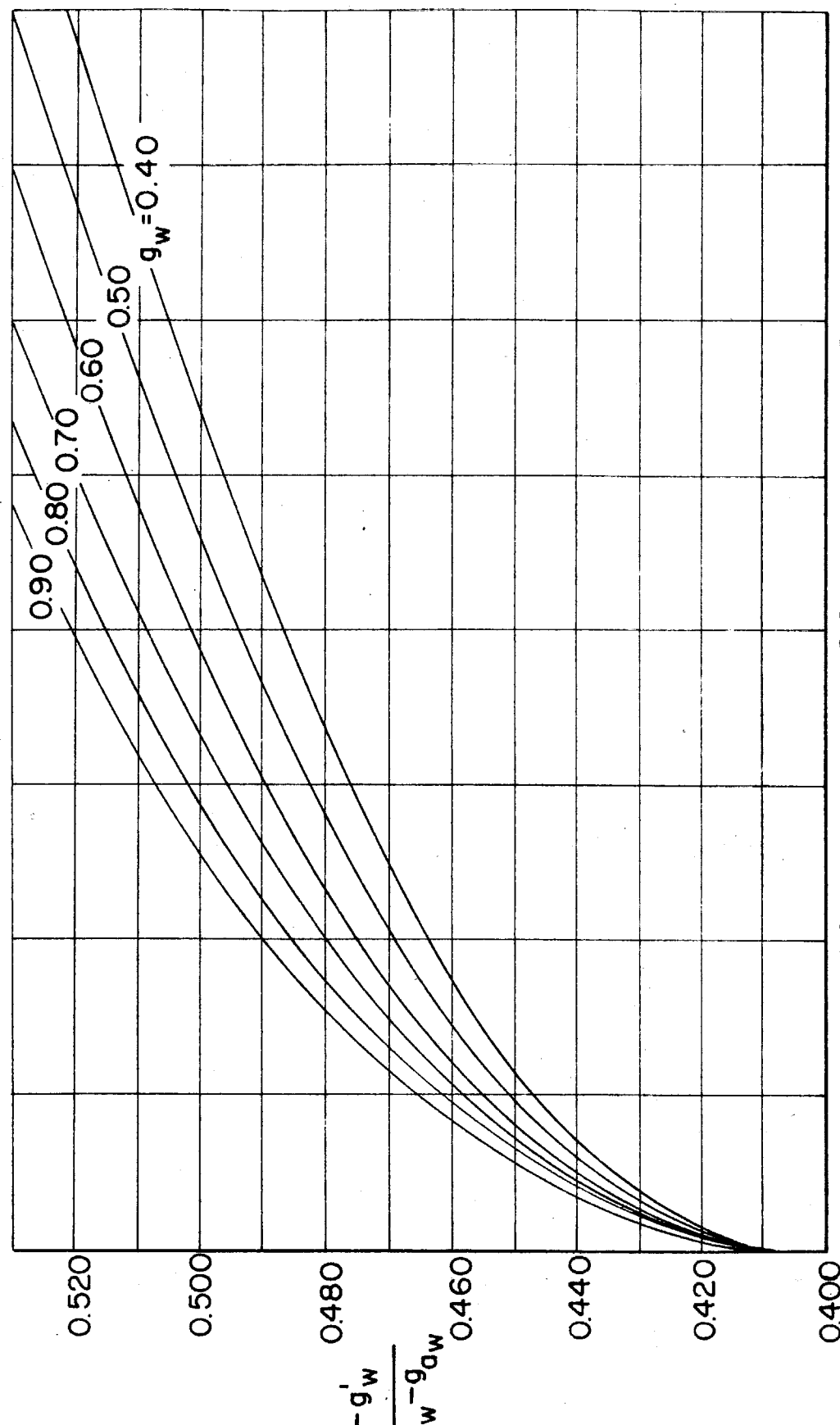

FIG. 27 – GRAPH OF INTERPOLATED DATA FROM REFERENCES 3,4 AND 7 FOR M=0, Pr=0.7